Recent nutrient enrichment and high biological productivity in the Labrador Sea is tied to enhanced winter convection

Jan-Erik Tesdal*†, Hugh W. Ducklow, Joaquim I. Goes

Lamont-Doherty Earth Observatory, Columbia University, Palisades, New York, USA

Igor Yashayaev

Department of Fisheries and Oceans, Ocean Sciences Division, Bedford Institute of Oceanography, Dartmouth, Nova Scotia, Canada

Corresponding author address: Jan-Erik Tesdal, Lamont-Doherty Earth Observatory, 61 Route 9W, Palisades, NY 10964

E-mail: jt7058@princeton.edu

†Program in Atmospheric and Oceanic Science, Princeton University, Princeton, NJ, USA

ABSTRACT

The Labrador Sea is known for strong surface heat losses and deep ocean ventilation in the wintertime as well as high biological productivity and carbon export associated with extensive spring blooms. Using satellite-derived estimates of ~~phytoplankton biomass (~~chlorophyll-a ~~)~~ and net primary productivity, this study documents that the Labrador Sea has recently become more productive, evident in the form of more intense and spatially extensive phytoplankton blooms. The spatial and temporal variability in chlorophyll-a was compared against trends in nutrient ~~variability to test the hypothesis that deeper mixing can be linked to large positive anomalies in phytoplankton biomass in recent years~~concentrations across the Labrador Sea. Nutrient concentrations were obtained on a repeat hydrography line running from the Labrador to Greenland shelves. The 25-year long time series of nitrate, phosphate and silicate concentrations along the AR7W line reveal decadal trends in the upper Labrador Sea. A comparison of these nutrients with basin-averaged annual mean surface chlorophyll-a concentrations reveals positive correlations in the upper 1000 m of the Labrador Sea. Furthermore, nutrient concentrations in the upper 1000 m were strongly correlated with wintertime convection depth. During years of strong winter convection, more nutrients are entrained from the deeper Labrador Sea, which then can be distributed through the Western Greenland and Irminger Currents and eddy activity, allowing sustained phytoplankton growth further north in the Labrador Sea.

1. Introduction

The subpolar North Atlantic (SPNA) has undergone dramatic change in the recent decade, notably large-scale freshening (Tesdal et al. 2018; Dukhovskoy et al. 2019; Holliday et al. 2020) and cooling (Robson et al. 2016; Piecuch et al. 2017), associated with intense heat loss to the atmosphere over the winter of 2013-2015 (Grist et al. 2016; Duchez et al. 2016; Yashayaev and Loder 2016, 2017) and a possible reduction in meridional heat and salt transport (Rahmstorf et al. 2015; Robson et al. 2016; Bryden et al. 2020; Tesdal and Haine 2020). Furthermore, a shift in subpolar gyre (SPG) circulation is apparent. Following a reduction of SPG size and weakening of its strength from the mid-1990s (Häkkinen and Rhines 2004; Hátún et al. 2017) there are clear indications of strengthening in the recent years (Tesdal et al. 2018). In addition to reduced salt influx from the south (Holliday et al. 2020), the continuing mass loss of the Greenland ice sheet (Dukhovskoy et al. 2019) and unprecedented sea-ice loss in the Arctic Ocean (Comiso et al. 2008; Parkinson and Comiso 2013) have increased freshwater fluxes into the SPNA. Underlying these recent freshening events is a more long-term freshening process, over the past 50 years, from an intensifying hydrological cycle and increased net precipitation in the SPNA (Dickson et al. 2002; Curry et al. 2003; Durack et al. 2012; Skliris et al. 2020).

These changes in ocean dynamics, heat, salt and freshwater transport raise questions about their biogeochemical and ecological implications for the SPNA, particularly the Labrador Sea and adjacent regions such as the Nordic Seas and mid-latitude North Atlantic. In the Labrador Sea, in particular, changes such as Greenland ice sheet melting can affect stratification and nutrient supply, both of which contribute to phytoplankton growth and overall productivity. For example, stronger phytoplankton blooms occurring in late summer could be due to a relief in iron limitation as a result

of additional iron input from glacial and iceberg melting (Arrigo et al. 2017; Hopwood et al. 2018, 2019), or to a alleviation of light limitation (Oliver et al. 2018).

In addition, one needs to take into account atmospheric variability. For example, Henson et al. (2013) attributed the anomalously large phytoplankton blooms in the Irminger Sea in summer 2010 to an extremely negative North Atlantic Oscillation (NAO) in the prior winter, which resulted in a shift in wind patterns. Unusually strong northerly winds brought additional freshwater and nutrients via the Labrador Current into the Irminger Sea, leading to an extended phytoplankton growing season (Henson et al. 2013). These one-year events are juxtaposed upon a presumed long-term decline in productivity in the SPNA (Osman et al. 2019). Thus, it is critically important to better understand variability in phytoplankton biomass and community structure in SPNA ecosystems and the multiple underlying processes that influence this variability, as ocean biology is subject to dramatic change as a consequence of changes in the physical state of the ocean.

Much work has gone into building our understanding of changes in the distribution of ocean phytoplankton. In high latitude oceanic ecosystems, such as the SPNA, efforts have relied on incomplete datasets of in-situ observations, but now are mostly aided by satellite ocean color data. Algorithms are applied to ocean color data to determine spatial and temporal variability in chlorophyll-a concentrations, a widely used proxy for phytoplankton biomass ~~(Yoder et al. 2010; Siegel et al. 2013)~~(Aksnesa and Ohman 2009; Yoder et al. 2010). Basin-scale observations of ~~phytoplankton biomass~~ chlorophyll-a using remote sensing began in the late 1970s, but it was not until the launch of NASA's Sea-viewing Wide Field-of-view Sensor (SeaWiFS) in 1997 that it became possible to collect a continuous global dataset of ocean color. Using the combined dataset from SeaWiFS and other advanced sensors, which now spans over 20 years, we have observed chlorophyll-a variability on seasonal, interannual, and decadal scales. However,

despite the availability of these data, the underlying causes and predictability of this variability remain limited (Siegel et al. 2013; Beaulieu et al. 2013; Henson 2014; Gregg and Rousseaux 2014).

In terms of bottom-up environmental factors~~influencing phytoplankton productivity~~, nutrient concentrations and light availability (with respect to the euphotic zone at 10-100 m water depth) are the dominant drivers of ~~chlorophyll-a variability~~phytoplankton productivity. Multiple studies suggest that in the tropics and temperate waters, increased stratification caused by ocean warming reduces productivity by reducing nutrient supply to the ocean surface (Behrenfeld et al. 2006; Polovina et al. 2008; Martinez et al. 2009). However, these findings are not directly relatable to higher latitudes such as the subpolar regions, where the response of phytoplankton growth to stratification is expected to be quite different. While the subtropical oceans are known to be limited by nutrient supply, the subpolar regions are widely believed to be mainly limited by light (Fay and McKinley 2017). In theory, greater vertical mixing would increase the vertical nutrient supply, but it would also increase light limitation by distributing phytoplankton populations over greater depths, thereby reducing photosynthetic rates.

Despite the in-situ data inadequacies, the SPNA is one of the most sampled ocean regions with a rich spectrum of studies in biological oceanography serving as the foundation for modern understanding of seasonal growth cycles in phytoplankton (e.g., Siegel et al. 2002; Behrenfeld et al. 2013; Westberry et al. 2016), interannual changes in phytoplankton biomass (e.g., Behrenfeld 2010; Harrison et al. 2013) and various mechanisms controlling these seasonal and interannual variations. The SPNA is also a region where clear connections between physical oceanography (i.e., circulation, vertical stratification and mixing processes) and biology have been reported (Barton et al. 2014; Hátún et al. 2016). While correlations between variation in physical conditions and phytoplankton biomass are consistently observed on a seasonal basis, they become much weaker at interannual to multidecadal timescales (Barton et al. 2014).

The SPNA is characterized by large seasonal phytoplankton blooms that represent distinct surges in ocean productivity occurring from winter to spring. The mechanisms that initiate and sustain the spring bloom include both top-down biological factors, such as grazing by zooplankton, and bottom-up environmental factors, such as nutrient and light availability (Behrenfeld and Boss 2017). Traditionally, it has been believed that the initiation of a spring bloom is associated with a critical depth of mixing, above which light conditions allow phytoplankton growth to exceed net losses such that the accumulation of biomass can occur (Sverdrup 1953). More recent work highlights the imbalance in predator-prey equilibrium as the crucial factor for bloom initiation (Behrenfeld 2010; Boss and Behrenfeld 2010). The revelation in the latter is that net positive growth in phytoplankton populations occurs well before the shoaling of the mixed layer in spring and instead occurs when the mixed layer is at its maximum depth. The underlying factor appears to be a decoupling of grazers from phytoplankton in a deepening mixed layer, which allows the phytoplankton population to increase (i.e., achieve a net positive accumulation rate).

Studies that focused on interannual and longer-term variability in SPNA phytoplankton blooms identified physical factors such as stratification, light and nutrient availability as the main drivers of the intensity of the blooms. For example, Martinez et al. (2016) found that chlorophyll-a concentrations in the mixed layers of the SPNA increased between the mid-1980s and mid-1990s. This change, observed in the eastern SPNA (east of 40°W between 50 and 60°N), corresponds to an increase in the abundance of diatoms and dinoflagellates. Across this same time period, a decrease in sea surface temperature (SST) and an increase in the mixed layer depth (MLD) were also observed. Martinez et al. (2016) suggest that deeper mixed layers may lead to enhanced nutrient concentrations in the upper layers, promoting higher phytoplankton growth during the spring and summer. However, it should be noted that nutrient data were not included in this work, so the

suggestion that nutrient concentration is a factor connecting phytoplankton growth and increased mixed layer depth is presented only as a speculative explanation for the trends observed in the data.

McKinley et al. (2018) observed different variability and trends in biomass over the SPNA. They observed a decline in phytoplankton biomass between 1998 and 2007 in the northeastern and southeastern (between 30-35°W) SPNA, which they associated with a reduced influx of nutrients into those regions. Phytoplankton biomass increased further west, in the central SPG south of Greenland, which was attributed to shoaling of the mixed layer and alleviation of light limitation. Unlike Martinez et al. (2016), who connected higher phytoplankton growth with deeper mixed layers and an increased nutrient supply in the SPNA, McKinley et al. (2018) points to higher phytoplankton growth due to shallower mixed layers. Also, Harrison et al. (2013) suggested that climate change will lead to progressively earlier and more intense spring blooms in the SPNA. They attributed this to the warming of the surface ocean leading to a more stable water column over the subpolar (and polar) oceans, which reduces light limitation (Doney 2006).

Another important physical factor that is believed to be linked to interannual changes in SPNA productivity is the horizontal SPG circulation, which modulates the distribution of nutrients (Hátún et al. 2016, 2017; McKinley et al. 2018). Hátún et al. (2016) showed that the strength and size of the SPG can influence zooplankton abundance in the northeast subpolar Atlantic by shifting the subarctic front eastward (i.e., closer to Reykjanes Ridge), bringing nutrients and fueling primary production. This establishes a causal link between the gyre variability and biological productivity in the eastern subpolar region. Furthermore, evidence suggests a link between the strength of SPG circulation and the availability of silicate, a key nutrient for diatoms, across the SPNA (Hátún et al. 2017). Changes in the SPG are associated with buoyancy forcing and wind stress over the SPNA (Häkkinen and Rhines 2004; Hátún et al. 2005; Foukal and Lozier 2017), which in turn

influence the depth of the mixed layer, providing another link between SPG and potential influences on primary production (Bennington et al. 2009).

The studies reviewed in the above paragraphs suggest that the variability of phytoplankton biomass, as well as the underlying mechanisms, can differ across the various regions of the SPNA. In the Labrador Sea for instance, the regulation of phytoplankton biomass and productivity appears to be unique, because deep vertical mixing during winter and SPG cyclonic circulation ensures an ample nutrient supply to support the high biological productivity (Harrison et al. 2013). Furthermore, the Labrador Sea is an important region of atmospheric carbon uptake (Körtzinger et al. 2008; Rhein et al. 2017). Sea ice melting and other freshening processes (e.g., melting of the Greenland Ice Sheet) also play an important role in the seasonal phytoplankton bloom dynamics of the Labrador Sea (Wu et al. 2008; Frajka-Williams et al. 2009; Frajka-Williams and Rhines 2010). Offshore advection of meltwater, eddy activity, and their effects on haline stratification appear to be responsible for the early blooms observed in the northern Labrador Sea (Frajka-Williams and Rhines 2010). On the other hand, in the central basin of the Labrador Sea, the initiation of the surface spring bloom coincides closely with the timing of the first cooling-to-heating shift in air-sea heat fluxes (Marchese et al. 2019). In regions like the Labrador Sea, wintertime convective mixing has been hypothesized to be a crucial player in determining the timing and intensity of spring blooms (Balaguru et al. 2018). The relationship between the winter mixed layer and spring blooms has been attributed to re-entrainment of sinking phytoplankton and reduced encounters with grazers, leading to decreased phytoplankton loss rates during the winter and increased accumulation during the spring. Other recent studies have described the impact of increased melting of the Greenland Ice Sheet on summer phytoplankton blooms and primary production, either from meltwater as a source of critical nutrients (e.g., iron) or from effects on stratification and light limitation (Arrigo et al. 2017; Oliver et al. 2018).

Here, we are examining the long-term variation of chlorophyll-a and primary productivity in the Labrador Sea over the last two decades and compare it with observed variability in nutrient concentration and wintertime convection. First, in Section 2, we describe the datasets and data processing methods used in this study. In Section 3, we then provide an overview of the variability in ~~phytoplankton biomass~~ chlorophyll-a over the entire SPNA allowing us to demonstrate that the Labrador Sea experiences unique variability in ~~phytoplankton biomass and primary productivity~~this parameter. Then, we present a description of nutrient distribution across a vertical section in the Labrador Sea based on in-situ observations, clearly showing that interannual variability in the upper layer nutrient concentration is a possible factor driving recent variability in ~~phytoplankton biomass~~ chlorophyll-a in the Labrador Sea. Finally, a relationship of Labrador Sea nutrient distribution and winter convection depth is demonstrated and discussed.

2. Data and Methods

Level 3 satellite chlorophyll-a concentration data were obtained from the NASA Ocean Color data center (`https://oceancolor.gsfc.nasa.gov`) as well as from the Ocean Productivity Group at Oregon State University (`http://sites.science.oregonstate.edu/ocean.productivity`). Both 8-day and monthly fields were obtained from SeaWiFS (1998-2010), Moderate Resolution Imaging Spectroradiometer Aqua (MODIS-Aqua; 2002-2018) and Visible Infrared Imaging Radiometer Suite (VIIRS; 2012-2018). The standard OCI algorithm was used for this study, but other algorithms are included for comparison (i.e., GSM and OCX). Furthermore, chlorophyll-a data were also retrieved from the GlobColour project, which provides a merged dataset from SeaWiFS, MODIS and MERIS (Medium Resolution Imaging Spectrometer). Modelled chlorophyll-a concentrations were obtained from the NASA Ocean Biogeochemical Model (NOBM; Gregg and Casey (2007)) and from the Pelagic Interactions Scheme for Carbon and Ecosystem Studies (PISCES,

Aumont et al. (2015)). NOBM output has been downloaded from the NASA Global Modeling and Assimilation Office (GMAO) and PISCES data from the Copernicus Marine and Environment Monitoring Service (CMEMS; `http://marine.copernicus.eu/`).

Monthly maps of net primary productivity (NPP) used in this study were obtained using four different productivity algorithms, which included the Vertically Generalized Production Model (VGPM) as well its Eppley variation (Eppley-VGPM), the updated Carbon-Based Productivity Model (CbPM2) and the Carbon, Absorption, and Fluorescence Euphotic-resolving model (CAFE). All of the satellite-based NPP data were obtained from the Ocean Productivity Group at Oregon State University, while simulated NPP were taken from the PISCES ocean biogeochemical model.

VGPM is a commonly used chlorophyll-based algorithm that estimates ocean NPP as a function of chlorophyll-a concentration, available light, and sea surface temperature. The Eppley variation (Eppley-VGPM) of this model (Behrenfeld and Falkowski 1997), which was utilized in this study, replaces the polynomial description of maximum daily NPP with an exponential function to determine the temperature-dependent description of chlorophyll-specific photosynthetic efficiencies. When comparing VGPM and Eppley-VGPM results, the interannual variability in NPP is very similar and the spatial distribution of the linear trends in NPP is identical. However, the overall higher values in VGPM are outliers compared to those from CbPM2 and CAFE, and for this reason Eppley-VGPM was used. The Eppley variation has the advantage of providing the same interannual variability and spatial trend as the original VGPM, while at the same time eliminating biases to yield output more in line with CbPM2 and CAFE. Hereafter, the Eppley variation of VGPM will be referred to as VGPM.

The CbPM2 algorithm estimates phytoplankton growth rate from chlorophyll-to-carbon ratios. The carbon estimate in the CbPM2 algorithm is derived from the amount of backscatter-derived particulate in the water column. CbPM2 describes NPP as the product of phytoplankton carbon

biomass and growth rate, rather than the traditional product of chlorophyll and photosynthetic efficiencies (Behrenfeld et al. 2005; Westberry et al. 2008). By incorporating carbon, the CbPM2 algorithm overcomes some of the limitations associated with using only chlorophyll, which has been shown to be strongly affected by the physiology and growth of phytoplankton under differing environmental conditions. The Carbon, Absorption, and Fluorescence Euphotic-resolving model (CAFE), also used for this study, is a carbon-based model that incorporates phytoplankton absorption. Unlike other carbon-based models that rely on chlorophyll-to-carbon ratios, the physiological assessments determined by CAFE are based on absorption-to-carbon ratios. CAFE calculates NPP as the product of energy absorption and the efficiency in which absorbed energy is converted into carbon biomass (Silsbe et al. 2016). We also include depth-integrated NPP estimates from the aforementioned PISCES biogeochemical model. Unlike the previously described satellite-based empirical models, PISCES simulates phytoplankton biomass as a prognostic variable (Aumont et al. 2015) from which NPP can be diagnosed.

This study also utilizes data from the regularly sampled Atlantic Repeat 7-West (AR7W) hydrographic line, which crosses the Labrador Sea between Hamilton Bank on the Labrador Shelf (53.5°N, 55.7°W) and Cape Desolation (60.7°N, 48.1°W) at the Greenland Coast. Stations along the AR7W transect were sampled in spring, from May through early June, in most years, with few exceptions in summer, from late June to mid-July (see Table 1). In-situ observations of silicate, nitrate and phosphate concentration along AR7W were collected by Bedford Institute of Oceanography (BIO) between 1994 and 2018 and made available through the Global Ocean Data Analysis Project version 2 (GLODAPv2, Olsen et al. (2016)). Nutrient observations for the year 2018 have been obtained directly from BIO. High-resolution temperature and salinity profiles were obtained from calibrated CTD data collected by BIO between 1994 and 2018. The nutrient concentrations

from bottle samples were overlaid on the higher resolution CTD casts at the matching stations along the AR7W hydrographic line.

All vertical profiles of the BIO shipboard dataset underwent extensive quality control. Preliminary analysis of physical and chemical variables along the AR7W line, suggest substantial year-to-year variations within deep water masses in the Labrador Sea. Given the fairly steady temporal variability in the deep ocean, these jumps or drifts in chemical concentrations are expected to be due to varying standard qualities and calibration methods between cruises. These inter-cruise changes are particularly large in the nitrate and phosphate concentrations. Therefore, cruise-dependent corrections have been applied to all three nutrients to improve temporal stability of the nutrient ratios in deep water masses of the Labrador Sea (i.e., Northeast Atlantic Deep Water). Details of this correction, including all steps of determining deep-water reference points, data processing and validation procedures, are is provided in Yashayaev et al. (2022). Given the larger correction factors in nitrate and phosphate, the interpretation of interannual nutrient variability is mainly relied on our analysis of in-situ silicate concentrations.

After processing and quality control, the in-situ observations were interpolated to a regular depth-distance grid in which distance from the Greenland coast was defined by taking a linear fit of the latitude and longitude of each station point for all AR7W cruises and then determining the intersection of that line with the Greenland coast. Data were first interpolated to discrete depth levels of variable resolution that correspond to in-situ sampling depths. The vertical resolution is 10 m in the upper 50 m of the section and incrementally increases up to 500 m at depth. The data was then linearly interpolated along the distance from Greenland at 10 km resolution. Profiles within the same 10 km distance grid cell were averaged before interpolation. No data extrapolation was performed to fill any grid cells lying outside of the outermost data points (e.g., above the shallowest data point, or next to the coast or seafloor).

Mixed layer depth (MLD) along the AR7W transect at the time of survey was derived from the BIO CTD dataset. Temperature and salinity were used to derive potential density (σ_0) profiles with 1-m vertical resolution, from which MLD was determined as the depth at which σ_0 is increased by 0.03 $\mathrm{kg\,m^{-3}}$ relative to σ_0 closest to the sea surface (z < 10 m). This MLD criterion has been shown to provide a reasonable representation of the mixed layer in regions where convection induces active turbulent mixing (Brody and Lozier 2015). This provided observation-based MLDs representative of the location and time of each profile. The winter MLD was also considered during March of each year, during which convective mixing is usually deepest in the Labrador Sea. Monthly fields of MLD from two global ocean reanalysis products were used. The first dataset was obtained from GLORYS12v1, which is a global ocean reanalysis with a spatial resolution of 12 km. Monthly fields from 1993 to 2018 were obtained from CMEMS. The second dataset of MLD fields is from the HYCOM GLBu0.08 reanalysis, obtained from the Ocean Productivity Group at Oregon State University for years 1998 to 2018. The original resolution of the HYCOM product is 12 km but has been regridded to 18 km resolution in the obtained dataset. For GLORYS12v1, the MLD criterion is the depth at which σ_0 increase compared to density at 10 m depth corresponds to a temperature decrease of 0.2°C. Similar to in-situ MLD, the chosen MLD criterion in HYCOM was based on a density threshold of 0.03 $\mathrm{kg\,m^{-3}}$ greater than at the surface. The gridded MLD fields from GLORYS12v1 and HYCOM were subsampled at the location of the AR7W hydrographic line to compare with nutrient data obtained in the May-July cruise of the same year. MLD from Argo profiling floats (Holte et al. 2017) were also included to compare to the reanalysis and shipboard-based MLD estimates.

In addition to the MLD, also included here is the aggregate maximum convection depth for each winter, as described in Yashayaev and Loder (2016). Hereafter referred to as convection depth, it is defined as the 75th percentile of the deepest reach of the pycnostad in the central Labrador Sea for

each winter. Density profiles were determined from Argo and available shipboard data over the winter months for each year. Trajectories of satellite-tracked surface drifting buoys from the NOAA Global Drifter Program were used to derive the mean surface circulation of the Labrador Sea. The trajectories were obtained from delayed-mode hourly data and real-time variable time-step data for the period 2000–2020. The drifter data were temporally interpolated into 15-min time intervals, binned into hourly bins, and low-pass filtered to remove tidal and inertial oscillations. Spatial binning into a 0.5° grid was done to obtain mean surface velocities. Monthly objectively analyzed fields of nitrate, phosphate and silicate concentrations were obtained for the newest release of the World Ocean Atlas (WOA 2018, Garcia et al. (2019)).

3. Results

a. Trends in chlorophyll-a over the subpolar North Atlantic

Monthly maps of chlorophyll-a from satellite as well as NOBM and PISCES models were used to calculate the linear trend at each grid point of the North Atlantic (Figure 1). All trends were evaluated on monthly anomaly data with seasonal cycle based on long-term monthly means removed. For consistency, we also looked at trends derived from annual average data, which revealed spatial patterns that are very similar to those derived from monthly anomaly data. Trends were derived for two defined 10-year periods, 1998-2007 (Figure 1a-c) and 2008-2017 (Figure 1d-f). This enabled comparisons between the two time periods and is based on correspondence with SeaWiFS data, which provides full annual coverage between 1998 and 2007, and latter half of MODIS data for the second period (2008-2017). Based on the comparison of trends between the two time periods, it is evident that the spatial patterns in some regions are clearly reversed between the two periods. A reversal from negative trends over 1998-2007 to positive trends in 2008-2017

is evident in the southeastern SPNA (Figure 1a, d). Between Iceland and Scotland and the area around Rockall Trough, we see a reversal from positive trends in 1998-2007 to negative trends in 2008-2017. Most of the Nordic Seas reverse from predominantly negative trends over 1998-2007 to predominantly positive trends over 2008-2017. On the other hand, the western SPG and Labrador Sea show positive trends for both time periods. Unlike the trend reversal in the southeastern SPNA, there is no clear reversal seen in the northeastern region south of the Nordic Seas (specifically, the Irminger Sea and Iceland Basin), where the trends are mostly negative over both time periods.

The spatial patterns in the satellite record are largely reflected in the NOBM dataset, however, they are reduced in magnitude (Figure 1b,c). In particular, the trend over 2008-2015 in the Labrador Sea is only slightly positive in NOBM compared to what is seen in the MODIS data, and there appears to be no trend in this region during 1998-2007. The spatial patterns in PISCES resemble very little of what is observed from the MODIS data (Figure 1c,f). The large-scale areas of positive trend in the eastern SPNA and in the central Labrador Sea are absent, and there is only a weak increase in the southern edge of the SPG. The only region where the linear trends derived from PISCES has some resemblance to the trends in the MODIS observations is in the Nordic Seas. However, the dipole pattern that is apparent in the simulated trends over the Nordic Seas during the 1998-2007 is not seen in the MODIS observations.

In summary, even though the spatial patterns of longer-term trends suggest chlorophyll-a increases in the Labrador Sea and the central subpolar region (Figure 1d), there are clear upward and downward trends that identify unique variability in distinct regions across the SPNA. While the Labrador Sea shows consistently positive trends, chlorophyll-a in the southeastern SPNA declined over the SeaWiFS period and increased over the recent 10 years, while in the northeastern part it declined during the SeaWiFS period, increased between 2003 to 2008 and then declined again after 2008.

On the other hand, focusing on the Labrador Sea and western SPG in general reveals positive trends in ~~phytoplankton biomass~~ chlorophyll-a that are consistent throughout the satellite record. In light of record deep convection in the Labrador Sea in recent years (Yashayaev and Loder 2017), one would expect increased light limitation in mixed layers, which is not consistent with the increased chlorophyll-a and productivity observed in the Labrador Sea during the same period. Balaguru et al. (2018) presented evidence of stronger April blooms in the northern Labrador Sea attributable to increased winter mixed layers. Also, the mixed layer in the spring can still be reduced due to increased freshening, despite the occurrence of deep mixing in the winter time. This increased spring and summer stratification can further enhance primary productivity due to alleviation of light limitation. Given persistently strong trends in the observed variability, which to some extent is reproduced by the model outputs, we, hereafter, will mostly focus on the Labrador Sea and its unique variability in ~~phytoplankton biomass~~ chlorophyll-a and productivity. Furthermore, possible mechanisms underlying the observed variability in chlorophyll-a in the Labrador Sea will be discussed.

b. Variability in ~~phytoplankton biomass~~ chlorophyll-a and productivity in the Labrador Sea

Given the unique character of chlorophyll-a variability in the Labrador Sea, we further focus on year-to-year differences by looking at monthly averages that retain the seasonality of each year. The monthly time series reveals large variation in the seasonality, including both timing and magnitude, of chlorophyll-a within the Labrador Sea (Figure 2a). The high chlorophyll-a values occur mostly in the northern half of the Labrador Sea off the Greenland coast, as seen in the annual mean distribution (determined over the MODIS period 2002-2018, Figure 2b). The timing of the annual chlorophyll maximum is consistent in the Labrador Sea, occurring in May with the exception of late peaks in July 2005 and 2017 and an early bloom in April 2018. Excursions are evident in

2014, 2015 and 2018, with peaks in previous years only half as high indicating that these extremely high excursions are recent phenomena. Regarding the 2018 excursion, it should be noted that the values for April are much larger in MODIS (ca. 5 $mg\,m^{-3}$) compared to VIIRS (ca. 2 $mg\,m^{-3}$) although both datasets show the same early peak in April.

The time series of monthly spatial chlorophyll-a averages in the Labrador Sea for 2002-2018 shows the annual peak occurring routinely in May, with slight shifts evident in 2005, 2017 and 2018 (Figure 2a). The extent of the annual bloom within the Labrador Sea was determined by mapping the May peak chlorophyll-a distribution for each year from 2002 to 2018 (Figure 3). Compared to most years, when maximum chlorophyll-a concentrations reach approximately 10-12 $mg\,m^{-3}$, a notably large phytoplankton bloom is evident in 2014 and 2015, with elevated chlorophyll-a concentrations over the entire Labrador Sea reaching as high as 30-50 $mg\,m^{-3}$. Strong interannual variability is also observed in the April through September mean distributions of chlorophyll-a concentrations (Figure 4). In addition to the large blooms in 2014-2015 that are similar to the May peak distribution shown in Figure 3, high annual means are also evident during 2016-2018, where unusually high chlorophyll-a concentrations were observed in other months (i.e., June-July in 2016 and 2017; April in 2018). The unique character of chlorophyll-a variability in the Labrador Sea is revealed in high values, particularly in recent years (i.e., 2014 to present), that extend over the entire basin rather than in particular locations (Figure 4).

Interannual variability in Labrador Sea ~~phytoplankton biomass~~ chlorophyll-a and productivity was further evaluated looking at area-averaged and integrated time series (Figure 5). Both area-weighted averages (Figure 5a) and area-integrals (Figure 5b) of the monthly fields were calculated over the Labrador Sea polygon (as indicated in Figure 2a), followed by averaging/integrating the monthly data from April through September (avoiding months where data is partly missing due to insufficient coverage). Here we include chlorophyll-a and NPP estimates from various

satellite-based (GlobColour, SeaWifS, MODIS and VIIRS) and model-based (NOBM and PISCES) data sets. Coverage now spans 21 years, from 1998 to 2018. We assume that the differences among the satellite products are largely due to values that are present in some datasets but missing in others, due to signal error (e.g., cloud cover) and variations in gap-filling between the different datasets. These differences are, with a few exceptions discussed below, mostly minor.

The overall variability in chlorophyll-a matches fairly well among the satellite data sets (grey and black lines, Figure 5a). Basin-wide spatial averages over the Labrador Sea show an increase between 1998 and 2003, which corresponds to what is seen in the spatial trends south of 60°N (Figure 1a). After 2003, the basin-wide average drops to a minimum of $\sim$0.6 mg m^{-3} in 2009. The first five years of the MODIS period (2003-2007) match very closely to the last five years in SeaWiFS. Over the entire time period 1998-2018, chlorophyll-a trends positive, but the most notable increases occur in the last ten years, with 2015 showing a record high ($\sim$1.0 mg m^{-3}). After the 2015 high, the satellite data are not in agreement, with the MODIS estimates considerably elevated and the VIIRS and GlobColour data indicating a return to pre-2014 values ($\sim$0.6 mg m^{-3}). Modelled chlorophyll-a data from NOBM and PISCES do not match well with satellite data, being generally lower in magnitude and demonstrating much weaker interannual variability (Figure 5a) without any sound resemblance with satellite observation.

Results from the analysis of chlorophyll-a concentrations ~~demonstrate~~ approximate the variability in phytoplankton biomass in the Labrador Sea. A measure of ocean productivity presented in the paper is net primary productivity (NPP), which describes the rate of organic matter production by phytoplankton. It is of interest to understand how spatial means and temporal variability of NPP in the Labrador Sea compare to those of chlorophyll-a, since NPP represents a more direct estimate of the amount of carbon available for higher trophic levels and export production. Monthly gridded fields of NPP were integrated over space and time from April through September to get

an estimate of total annual production (in Tg) during each year in the Labrador Sea (Figure 5b). Given the lack of satellite data during the winter months, the annual estimate is based on months April through September. Overall satellite-based productivity models (VGPM, CbPM2 and CAFE) show consistent variation in annual production that is similar to what is seen in the annual mean chlorophyll-a. Annual production from PISCES matches the overall mean across all estimates (at around 30 $\mathrm{Tg\,C\,yr^{-1}}$), but shows very little year-to-year variation and no similarity to the satellite based estimates, as expected from the comparison of observed and modelled chlorophyll-a distributions and trends presented above.

Integrated production derived from all three productivity models suggest an overall increase over the latter half of the MODIS time period (2012-2018), following a decline from 2002-2009 and a spike in annual production in 2010. The 2010 peak in productivity is particularly notable in VGPM and CbPM2, and matches well with the observed chlorophyll-a peak. CAFE has generally higher estimates and less of a long term trend than what is seen with VGPM and CbPM2, which clearly show higher values in recent years (2015-2017) compared to earlier periods. Production derived from CbPM2 is generally lower compared to VGPM. This is consistently the case for both the SeaWiFS and VIIRS datasets. Despite a shift in the absolute values, both algorithms result in a long term positive trend for the Labrador Sea. Estimates show some variation among the SeaWiFS, MODIS and VIIRS sensors. In the case of CbPM2-derived production, SeaWiFS and VIIRS consistently estimate lower values than MODIS. Despite the shifts among the sensors and different algorithms, Figures 2-5 clearly indicate that the Labrador Sea has recently become more productive, with greater and more spatially extensive phytoplankton blooms. In the next section, in-situ data in the Labrador Sea are used to seek possible relationships with the observed variability in ~~phytoplankton biomass~~ chlorophyll-a in the Labrador Sea in recent years.

c. Nutrient concentrations along the AR7W transect

Observational data were obtained from the Atlantic Repeat Hydrography Line 7 West (AR7W), a vertical transect across the Labrador Sea that is sampled at least annually during May to July by the Bedford Institute of Oceanography as part of the World Ocean Circulation Experiment (WOCE) since 1990. Data for 1994 to 2018 were used in this analysis (Table 1). The AR7W line crosses varying biogeographic and hydrographic zones (Figure 6), including shelf, slope and deep water regions with varying regimes of haline and thermal variability and stratification, which shape the composition and seasonality of phytoplankton communities (Fragoso et al. 2016). As the chlorophyll-a satellite data record begins in 1998, the AR7W data covers the entirety of the period discussed in the previous section. For the most part, AR7W cruises occurred between May and June of each year, and despite the varying sampling time over a six-week window, the data are assumed to consistently represent late spring to early summer conditions. The exceptions are the years 1998, 1999, 2002 and 2003, during which the cruises happened in July. Observations sampled during those years likely reflect a different seasonal state of the nutrient field, and therefore are excluded for some of the analysis as they are less comparable to other years. There are a few instances of missing data because in several cruises, nitrate (i.e., 1994, 1998-2001, 2003, 2013) and phosphate (i.e., 2002) observations did not meet initial quality control requirements. Silicate measurements are more robust to chemical standards and analytical calibration inconsistencies and thus are available for all cruises. Because of cruise cancellation, sampling along the AR7W transect did not occur in 2017.

The analysis of nutrient concentrations focused on silicate, nitrate and phosphate to determine if any variations along the AR7W line could be correlated with the chlorophyll-a time series discussed previously (Figures 2a and 3). The in-situ observations of the three nutrients were interpolated

onto a regular depth-distance grid along the AR7W hydrographic line (Figure 6). Any data points that were located farther than 10 km from the line were excluded. The mean vertical nutrient distribution across the AR7W transect from 1994 to 2018 reveals a sharp vertical gradient in the upper ocean (at $\sim$50 m, Figure 7). It also shows a clear gradient across the basin, with lower values to the northeast, towards the Greenland coast. The mean near-surface concentrations for nitrate are 5 to 10 $\mu mol\,kg^{-1}$, 0.3-0.8 $\mu mol\,kg^{-1}$ for phosphate and 2-5 $\mu mol\,kg^{-1}$ for silicate, with more depleted values for each nutrient occurring closer to Greenland.

Climatological nutrient fields from WOA 2018 are subsampled to describe the mean annual cycle and determine wintertime maximum nutrient concentrations in the upper 20 m of the AR7W transect (excluding the Labrador Shelf). The point of this exercise was to gain an understanding of nutrient changes as phytoplankton enter their springtime growth phase and clarify the drawdown for each nutrient and the potential for nutrient limitation. The mean climatologies for silicate, nitrate and phosphate were compared to the AR7W dataset for 1994-2018 (Figure 8). Upper nutrient concentrations were assumed to be at their maximums during winter and estimated as the concentration at the depth of the mean winter MLD (Glover and Brewer 1988). Here we choose the March value from the Argo MLD climatology of Holte et al. (2017). It is evident that by the time of the annual cruises (i.e., May-July), there has already been substantial drawdown for each nutrient, especially in the top 200 m layer. However, none became limiting as they are all on average above their half saturation concentrations. One exception are the July cruises in 1999, 2002 and 2003 which indicate limiting silicate concentrations (below 2 $\mu mol\,kg^{-1}$, Egge and Aksnes 1992). The error bars indicate the spread of the 1994-2018 values and leaves the possibility of years or specific regions where nitrate or phosphate become limiting. On average, nitrate and phosphate are taken up in the same ratio (N:P = 15:1) over the annual cycle and remain in excess. On the other hand,

silicate is low relative to nitrate (i.e., Si:P = 8:1 and Si:N $\approx$ 1:2) and is more likely to become limiting, especially close to Greenland (Figure 7).

In the intermediate depths between approximately 200 and 1000 m, nutrient concentrations are much more homogeneous. Nitrate ranges from 15 to 16 $\mu mol\,kg^{-1}$, phosphate is approximately 1 $\mu mol\,kg^{-1}$ and silicate ranges from 8 to 9 $\mu mol\,kg^{-1}$. The vertical distribution of nutrient concentrations show a clear first-order alignment with density contours (Figure 7), indicating that the deep nutrient pool in the Labrador Sea follows water mass distributions. Nitrate and phosphate concentrations reach their maximum levels (16-17 $\mu mol\,kg^{-1}$ and 1.1 $\mu mol\,kg^{-1}$, respectively) at a σ_0 range of 27.76-27.82 $kg\,m^{-3}$, corresponding to the range of the Labrador Sea Water (LSW) classes produced between 1987 and 2019 (Yashayaev 2007; Yashayaev and Loder 2016, 2017). By contrast, silicate maximum values of 12 to 13 $\mu mol\,kg^{-1}$ are observed at σ_0 range 27.82-27.88 $kg\,m^{-3}$, coinciding with the Northeast Atlantic Deep Water (Yashayaev 2007).

Anomaly fields were derived by subtracting the 2004-2016 mean from the 2004-2006 mean (Figure 9a-c), and from the 2014-2016 mean (Figure 9d-f). These three-year periods of the AR7W dataset were chosen to illustrate the change in nutrients over the time period and to only include years in which sampling occurred between May and June. As described above, data from cruises prior to 2004 were excluded from the analysis because they occurred later in the summer and reflect a different seasonal state of the nutrient field (i.e., more depleted). The three-year periods also correspond to years with low chlorophyll-a (2004-2006, Figure 2a) and with relatively high chlorophyll-a (2014-2016, Figure 2a). The 2004-2006 nutrient concentrations are generally less than the overall mean (i.e., mean of 2004-2016) and the anomaly is more pronounced in the upper 50 m of the central Labrador Sea (Figure 9). Conversely, nutrient concentrations during 2014-2016 are generally greater than the overall mean. During this period the anomalies are pronounced over the upper 50-100 m of the central basin, as well as the upper 50 m close to Greenland and over

the Labrador shelf (Figure 9d-f). Positive anomalies are observed deeper in the ocean during both time periods, whereas the differences between 2004-2006 and 2014-2016 are only clear in the upper 50-100 m. As chlorophyll-a and NPP are generally greater during the 2014-2016 period, this suggests the positive nutrient anomalies in the upper Labrador Sea are associated with enhanced phytoplankton growth and productivity.

The mixed layer depth (MLD) along the transect was determined by using vertical profiles of potential density anomaly (σ_0), with MLD defined as the depth at which the potential density anomaly exceeds 0.03 $\mathrm{kg\,m^{-3}}$ greater than the surface value. The black lines in Figure 9 denote the MLD corresponding to each time period. The mean May-June MLD is shallow towards the shelves and reaches a maximum of 300 m in the central Labrador Sea. The deeper MLDs coincide with higher nutrient concentrations in the upper layers (Figure 7). The negative nutrient anomalies in the upper 50 m during 2004-2006 coincide with a shallower MLD across the basin, while the positive nutrient anomalies during 2014-2016 coincide with a generally deeper MLD in the central basin (Figure 9). This is consistent with the concept that deeper MLDs are associated with greater vertical nutrient flux to the upper layers of the ocean.

The mean silicate-to-phosphate (Si:P) ratio along the AR7W transect is between 8:1 and 9:1 (Figure 10a), which is clearly below the 15:1 ratio that is expected from diatom composition (Brzezinski 1985). The Si:P ratios also show spatial heterogeneity in the upper 200 m. In the upper 50 m close to Greenland, and in the central Labrador Sea, lower Si:P ratios of 6:1 to 7:1 are evident. In some offshore regions approximately 150 km from Greenland, ratios reach as high as 10:1. Waters over the Labrador Shelf also exhibit higher Si:P ratios of around 10:1. For the nitrate-to-phosphate (N:P) ratio, the mean in the central Labrador Sea is close to the Redfield ratio of 16:1, but shows lower values between 6:1 and 9:1 close to the surface, especially near the Greenland coast and over the Labrador Shelf (Figure 10b).

The anomalies in Si:P ratios of the first (Figure 10c) and last (Figure 10e) three-year period show similar patterns to the anomalies in silicate alone (Figure 9a, d). This suggests an enrichment in silicate that is not mirrored by phosphate. Furthermore, these anomaly patterns are not as strong in the case of the N:P ratio (Figure 10d, f). Whereas the Si:P ratio increases over the entire upper Labrador Sea in 2014-2016, N:P ratios increase only near the Greenland coast and in the surface waters at the southwestern end of the AR7W transect. Also, the Si:P ratios show clear negative anomalies over 2004-2006, while the N:P ratios do not.

d. Relationship between ~~phytoplankton biomass~~ chlorophyll-a and nutrients

Satellite estimates of chlorophyll-a for the years 2004-2006 show relatively low chlorophyll-a concentrations over the Labrador Sea, while years 2014-2016 are associated with high chlorophyll-a concentrations and exceptionally large blooms in May 2014 and May 2015 (Figure 2a). To determine whether chlorophyll-a variability on the Labrador Sea can be associated with variability in nutrients observed along the AR7W transect, Pearson correlation coefficients were calculated between the annual spatial average of chlorophyll-a for the Labrador Sea (region outlined in Figure 2b) and the nutrient concentrations for each grid point of the AR7W transect (Figure 11). The nutrient concentrations for each grid point are correlated with the same spatial average of MODIS chlorophyll-a, which represents values for the sunlit surface.

The distribution of correlations over the vertical transect shows that annual mean chlorophyll-a over the Labrador Sea is positively correlated with springtime nutrient concentrations. This is true along the entire transect in the upper 1000 m, especially in the central Labrador Sea. The three regions that show the greatest correlation are in the southwest around the Labrador Current, in the center of the deeper Labrador Sea (between 200 to 1000 m), and centered in the West Greenland Current, where significant positive correlations are evident for silicate and nitrate (Figure 11a-

b) but not for phosphate (Figure 11c). For phosphate, there are only weakly positive values in the central Labrador Sea (upper 1000 m and close to Greenland~~. Concentrations~~). Nutrient concentrations in the deep ocean between 1000 to 2000 m show consistently negative correlations with surface chlorophyll-a. The negative correlation at these depths suggests that in years when winters are associated with particularly deep mixing (> 1000 m), the upwelling of nutrients reduces their concentrations in the deep ocean and increases concentrations in the surface layers, thereby supporting increased productivity over the following summer.

The correlations pattern in the upper 100 m is different for silicate compared to nitrate and phosphate (Figure 11). Silicate concentrations tend to be higher near the surface during years of elevated chlorophyll-a concentrations. On the other hand, both nitrate and phosphate exhibit some negative correlations with annual chlorophyll-a in the upper 200 m. Here, we are mostly interested in the amount of nutrients that is available throughout the growing season in a given year. Thus, we focus on the nutrient concentrations below 200 m and above 800 m, which has been less affected by drawdown by the time of the cruise (Figure 8). Given the higher fidelity in silicate measurements (Yashayaev et al. 2022) and the covariability of average nutrient concentration in the Labrador Sea between 200 m and 800 m depth (Figure 12), we will focus on silicate as ~~as~~ a proxy of nutrient availability.

e. Relationship between nutrients and MLD along the AR7W transect

The MLD has been shown to be an important indicator of stratification, which affects phytoplankton growth both directly (by reducing light limitation) and through its impact on surface nutrient concentrations. The interannual variability in nutrient data along the transect can be directly compared against the MLD using the AR7W data. Figure 13a shows the correlation pattern between the local MLD and silicate at each set distance point during the May-July sampling period. In

the upper 100 m of the central Labrador Sea, positive correlations are observed between silicate concentration and the MLD. Below 100 m, these correlations are negative, suggesting that deeper MLDs are associated with an increase in nutrient supply that is seen over only the upper 100 m of the central Labrador Sea, and the upper 20-50 m over the Labrador shelf. These correlations are much weaker close to the Greenland coast, which suggests that silicate concentrations are less connected to the MLD in that area.

There is notable spread in the Argo observations surrounding the AR7W transect, indicating that MLDs are spatially heterogeneous in that region. Considering this spread, there is fairly good agreement between Argo MLDs and those derived from BIO AR7W CTD data (Figure 14). A comparison with MLDs from high-resolution reanalysis fields (GLORYS12v1 and HYCOM) shows general agreement in terms of the overall spatial variation along the AR7W transect in May. However, the extent and details of MLD variation are quite different for each data product. In particular, the two reanalysis products demonstrate notable differences in their representation of MLD variation and only limited agreement with observations. Consequently, no particular reanalysis product can be judged to represent MLD variability in the Labrador Sea better than the others.

In order to seek correlations between the deeper March MLDs and May AR7W silicate concentrations, it was necessary to use MLD from reanalysis products. Given the general disagreement in MLD values across reanalysis products (Figure 14), we include the March MLD from both reanalysis datasets, HYCOM and GLORYS12v1 (Figure 13b). Positive correlations between the March MLD from HYCOM and May silicate concentrations are observed below the seasonal MLD ($\sim$100 m) over the central Labrador Sea. When March MLD are taken from GLORYS12v1, we see significant correlations in the upper 100 m of the central Labrador Sea. The overall correlation pattern in the central Labrador Sea between silicate concentrations and winter mixing is in accordance

with the notion that a deep water column is associated with nutrient rich water. However, no such correlation pattern is observed near the Greenland coast. Thus, locally higher silicate concentrations are not associated with deeper winter mixing in the upper water close to Greenland. It is only further offshore that deeper winter mixing is associated with greater silicate concentrations.

Positive correlations between the MLD and silicate concentrations in the upper 50 m are observed only in the central Labrador Sea, suggesting that nutrient concentrations off the Greenland coast are affected by a mechanism other than vertical supply through winter mixing. The absence of any significant correlation between silicate and MLD off the coast of Greenland does not support a direct link between vertical supply and high silicate concentrations in the upper waters of that region. On the other hand, the overall circulation regime (Figure 6) allows nutrients (especially silicate) to be transported through the boundary currents sourcing from the Arctic Ocean, along the East and West Greenland Current, and on into the northern Labrador Sea. It has been suggested that the SPG regulates silicate concentrations in the North Atlantic (Hátún et al. 2017), indicating that by comparing SPG strength indices against silicate concentrations it is possible to assess the relevance of gyre strength on nutrient transport off the Greenland coast.

f. Relationship between nutrients along the AR7W transect and gyre strength

Satellite altimetry provides a decadal long record of SPG strength variability, from 1993 to the present. Daily gridded fields of the multialtimeter absolute dynamic topography product were downloaded from the Copernicus Marine and Environment Monitoring Service (CMEMS; `http://marine.copernicus.eu/`). The daily fields were selected for the period 1993-2018 and averaged to monthly mean fields. Absolute dynamic topography is referred to here as sea surface height (SSH). The Subpolar Gyre Index is defined as the principal component of the second

Empirical Orthogonal Function (Koul et al. 2020) (i.e., second principle component), but here is derived using monthly anomalies of SSH over the North Atlantic (20°N to 70°N, 0°W to 80°W).

The time series of the gyre index (Figure 15) indicates that SPG strength was at a maximum in the early to mid 1990s (Häkkinen and Rhines 2004). After a period of decline, as documented by several studies (Häkkinen and Rhines 2004; Hátún et al. 2017), SPG strength reached another, almost identical maximum in 2016 (Figure 15). It was therefore deemed relevant to test the connection between gyre strength and Labrador Sea silicate concentrations for the longer time period (1994 to 2018).

A composite analysis was used in which years of a "strong gyre" are defined as those in which the gyre index exceeds one standard deviation above the mean, and years of a "weak gyre" as those in which the gyre index exceeds 1 standard deviation below the mean. This is illustrated in (Figure 16) as the normalized gyre index, where the PC2 of SSH has been normalized (by subtracting the mean and dividing by the standard deviation). It should be noted that this analysis, based on the longer time period 1994 to 2018, includes sampling periods for silicate concentration that range from from May to July in the years prior to 2004, whereas sampling after 2004 occurred during May to June (Table 1). Therefore some variability may be attributable to seasonal rather than interannual variation.

For strong SPG years, average silicate concentrations across the transect field are found to be higher than average over the entire deep basin, especially in the upper 100 m (Figure 17a). For weak SPG years, average silicate concentrations are above the mean only in the upper 50 m towards the Labrador Shelf (Figure 17b). In years of a strong SPG, but not in years of a weak SPG, silicate concentrations have positive anomalies present close to the Greenland coast, where circulation is directed northwest via the West Greenland Current. A similar picture occurs when plotting the anomaly distribution of Si:P ratios for years of strong (Figure 17c) and weak (Figure 17d)

SPG, reflecting an enrichment in silicate compared to phosphate. This suggests that increased nutrient concentrations in the upper layers of the Labrador Sea can be attributed to an enhanced SPG strength. However, the relative importance of convective mixing versus horizontal (i.e., gyre-driven) circulation in regulating blooms is yet unanswered. The following section accounts for the importance of deep winter convection in bloom dynamics in the Labrador Sea.

g. Relationship between nutrients along the AR7W transect and convection depth

As noted above, the spatial pattern in MLD is very heterogeneous over the Labrador Sea and across the AR7W transect associated with large temporal variability and uncertainties. Especially, winter MLDs are difficult to accurately estimate due to sporadic observations. Therefore, an estimate of the aggregated convective depth, which represents the overall extent of wintertime deep convection in a given year, is used here to further test the relationship between vertical mixing and nutrient supply in the Labrador Sea. An annual time series of convection depth is derived using vertical profiles of σ_2 (i.e., potential density anomaly with reference pressure of 2000 dbar) from available Argo and shipboard profiles over the course of the entire winter. Deep convection in the Labrador Sea is characterized by decadal variability that closely matches variability in SPG strength (Figure 15). Both deep convection and gyre strength appear to have intensified in the recent years, consistent with findings by Yashayaev and Loder (2017).

The correlation of convection depth with silicate, nitrate and phosphate concentration was evaluated for each grid point of the depth-distance grid along the AR7W transect over the time period 1994 to 2018 (Figure 18). The correlation analysis between convection depth and nutrient concentration is on a year-to-year basis. As defined in our study and described in Yashayaev and Loder (2016), convection depth represents the integrated impact of vertical mixing over the winter and is presented here as an annual time series. Similarly, the nutrient time series are presented as

annual time series for each grid point and represent the concentration at the time of the cruise, which usually occurred in May-June, with a few exceptions of sampling in July. In the top 50 m layer, the seasonal cycle is likely to dominate the variability of nutrients, biasing the respective correlation. However, a clear positive correlation between convection depth and nutrient concentrations below 50 m and above 1000 m of the Labrador Sea is most likely reflective of a real connection between convection and nutrients. Correlations are particularly strong in the case of silicate (Figure 18a) with weaker correlations in nitrate (Figure 18b), while phosphate shows very little positive correlations with convection depth (Figure 18c). Furthermore, there are clear negative correlations between convection depth and nutrient concentration below 1000 m across the section. This suggests a physical redistribution of the deep Labrador Sea nutrient pool to the upper water column by deep winter mixing.

The positive relationship between silicate concentration in the upper Labrador Sea and convection depth is particularly striking. Correlations are more pronounced at the intermediate depths, in the layer of the ocean less affected by seasonal cycle aliasing with interannual variability. This corresponds to be below the seasonal mixed layer during the time of sampling, whose 1994-2018 mean shows it at $\sim$50 m towards the shelf and at $\sim$150 m in the central Labrador Sea (Figure 7). This highlights an important fact – nutrient concentrations in the surface layer of the Labrador Sea experience strong seasonal variability affecting the annual survey data randomly positing anywhere between the first days of May and mid-June. An annual time series representing interannual variability in upper silicate concentration is derived by taking the average over a depth from 200 to 800 m across a half of the AR7W section adjacent to Greenland (i.e., $\sim$100-450 km off Greenland). The reasoning for selecting this particular part of AR7W is that this region is likely to be affected more strongly by the northwestward-flowing Irminger and West Greenland currents, where light conditions due to freshwater-induced stratification are beneficial to phytoplankton growth and

where blooms are usually occurring (Figure 4, Frajka-Williams and Rhines 2010; Lacour et al. 2015; Marchese et al. 2019). The averaged silicate concentration covaries with the annual mean chlorophyll-a concentrations and both are significantly correlated with convection depth (Figure 19). These relationships support the idea that deep convection enriches the upper Labrador Sea in nutrients. This is likely dominant only below 200 m, with consideration of Arctic sources necessary at the surface, but the overall effect is to allow more extensive phytoplankton blooms throughout the growing season.

4. Discussion

This study has shown that winter convection plays an essential role in redistributing nutrients in the top two kilometers of the water column in the Labrador Sea. Positive correlations between nutrient concentrations and convection depth occur in the upper 1000 m of the Labrador Sea. This demonstrates that entrainment of nutrient-rich waters prevails over mixing of depleted waters during winters in which convection depth is enhanced, and in turn results in a greater nutrient supply to fuel larger phytoplankton blooms over the growing season. Conversely, during winters in which convection depth is weaker, a net loss of nutrients in the upper Labrador Sea is expected. In years prior to weak winter convection, nutrient uptake from phytoplankton growth and subsequent sinking of organic material predominates, leading to a net transfer of nutrients into the deeper ocean, which in turn reduces nutrient availability during spring and summer of the following year.

The correlation pattern across the AR7W transect of silicate, nitrate and phosphate with convection depth are consistent but show clear differences in that the silicate-convection correlation is stronger and more extended over the section. This discrepancy could be explained by the difference in the mean vertical distribution of the three nutrients (Figure 7). Whereas nitrate and phosphate concentrations are almost at their highest concentrations (i.e., 15 to 16 $\mu mol\,kg^{-1}$ and $\sim$1 $\mu mol\,kg^{-1}$,

respectively) at intermediate depth levels of 100-200 m with very little increase below that, silicate concentrations display a clear vertical gradient that reaches a maximum concentration situated much deeper (∼3000 m) compared to nitrate and phosphate maximums at 1500-2000 m. As convection depth ranges from 630 to 2300 m, and nitrate and phosphate concentration are fairly homogeneous below 200 m, the vertical redistribution of nutrients due to changes in winter convection should affect silicate much more than nitrate and phosphate. Possible differences in the sinking rates of diatom shells (i.e., opal) and other inorganic and organic material, as well as differences in remineralization of silicate from opal versus nitrate and phosphate from non-siliceous material, could explain the relatively low silicate concentrations at intermediate depths of the Labrador Sea. However, it is not apparent that remineralization of opal is less pronounced compared to non-siliceous materials (Thomalla et al. 2008).

The relationship between winter MLD from reanalysis products and silicate concentration (Figure 13b, c) were not as clear as the one demonstrated between silicate and winter convection depth (Figure 18a). This may be attributable simply to reanalysis data not sufficiently reflecting observations, but it may also be due to differences between the aggregated effect of deep water formation (i.e., Labrador Sea Water) and local mixing, which shows pronounced spatial and temporal variability. For example, the vertical movement of the pycnocline due to mesoscale eddies can have a large influence on winter MLD (Gaube et al. 2019), but this should not impact the year-to-year variability of winter convection. Therefore, convection depth appears to be a better reflection of the wintertime redistribution of nutrients between depleted surface waters and nutrient rich deep water in the Labrador Sea.

The convection depth is correlated with gyre strength (Figure 15). Using the annual time series of the sea surface height based index, representing SPG strength, instead of convection depth shows that enhanced silicate concentrations (and higher Si:P ratios) in the upper 1000 m across the AR7W

section occurs in years of a strong SPG, and also anomalously lower values in years of a weak SPG (Figure 16 and 17). This relationship between silicate and gyre strength matches the findings of Hátún et al. (2017), who observed declining silicate concentrations throughout the SPNA over the period 1990-2015.

Declines of 0.55-0.66 μM per decade were observed in the central Labrador Sea, the northern Irminger Sea, and the Nordic Seas. Struck by the remarkable consistency of the decline across the SPNA, Hátún et al. (2017) used the gyre index to connect the decline in silicate concentration with a weakening SPG. In our study, a revised, detrended gyre index is used (Koul et al. 2020), which suggests an increase in the gyre strength from 2014 onwards, coincident with increasing silicate concentrations in the Labrador Sea. Expanding on and extending the work of Hátún et al. (2017), the work described here demonstrates a positive correlation between SPG strength and silicate concentrations in the Labrador Sea in recent years.

However, due to the strong relationship between the SPG strength and the deep convection in the winter (Figure 15), this study points out that it might not merely be horizontal advection as the cause of decreases or increases in nutrient concentrations, but that vertical supply of nutrients through winter convection might also play an important role. While the size and circulation strength of the SPG may influence silicate distribution in the North Atlantic as a whole, this study suggests winter deep convection as a key driver specific to the Labrador Sea. Furthermore, increased deep convection is likely the driver for the recent strengthening of the SPG as the deepening of the isopycnal surface and reduced stratification lead to greater baroclinicity in the SPG. Based on general circulation patterns in the Arctic and subpolar North Atlantic, previous work postulated that productivity in the subpolar regions is dependent on silicate-rich waters of Arctic origin arriving via the East Greenland Current (Tremblay et al. 2002; Torres-Valdes et al. 2013). While this may be the case for the boundary region, the present study points out that winter convection is the major driver

for nutrient replenishment in the central deep basin. For example, the recent increase in silicate concentration is detected throughout the upper 1000 m (Figure 9d) as well as spatially correlated with the winter convection depth (Figure 13a) in the Labrador Sea. However, Arctic water masses are expected to reside only in the upper 200 m of the Labrador Sea (Frajka-Williams and Rhines 2010; Torres-Valdes et al. 2013), which does suggest that the recent silicate enrichment is not of Arctic origin. Additionally, the boundary flow is rather compact with strong closely positioned recirculating flows.

The connection between deep convection and vertical nutrient supply is potentially an important factor in phytoplankton biomass and biological productivity in the Labrador Sea, as this study has shown that annual mean ~~biomass~~ chlorophyll-a measured by satellite is connected to nutrient concentration in the upper Labrador Sea. Generally, nutrient enrichment leads to greater dominance of diatom growth (Armbrust 2009), such as it has been detected during the North Atlantic spring bloom (Weeks et al. 1993). An open question is what nutrient eventually is limiting the phytoplankton blooms. Our preliminary analysis suggests that the Labrador Sea is relatively depleted in silicate as early as in springtime (Figure 8). Whereas at depth nitrate and phosphate are in accordance to the Redfield ratio of 16:1 (Figure 10a), the silicate to phosphate ratio is only 8:1 (Figure 10b), clearly below the expected 15:1 ratio.

Silicate depletion is also evident in the negative values of the Si* tracer (where Si* = Si - N) throughout the AR7W section, indicating that the Labrador Sea is deficient in silicate relative to nitrate according to the typical understanding of diatom growth (Ragueneau et al. 2000; Brzezinski 1985; Brzezinski et al. 2002; Sarmiento et al. 2004). Therefore, with sufficient nitrate and phosphate, the diatom blooms during spring most likely ceases due to a deficit in silicate. This is in accordance to a recent study that showed the depletion of silicate occurring before nitrate and identified it as the main factor in terminating the spring bloom (Krause et al. 2019). As the diatom bloom

abates, nitrate and phosphate should still be sufficient to allow elevated biological production in summer and fall. While some studies have investigated changes in phytoplankton community composition in relation to generalized physical distinctions between North Atlantic and Arctic regions (Fragoso et al. 2016, 2017, 2018) there is potentially great benefit in documenting shifts in species compositions as they relate specifically to spatial and temporal variation in nutrient availability and how this affects the marine ecosystem and carbon export.

In order to understand the connection between enhanced phytoplankton growth and vertical supply of nutrients it is important to consider the predominant circulation patterns along the Greenland side of the Labrador Sea. Regions of high chlorophyll-a are located further northwest of the AR7W transect off the Greenland coast (Figures 2b, 3 and 4). It is likely not only the local nutrient concentration that affects productivity at that location, but also input through horizontal advection. For example, positive concentration anomalies in the upper 50 m silicate concentrations close to Greenland were observed during the period 2014-2016 (Figures 9d-f). These were likely due to stronger winter convection resulting in an enrichment of upper nutrients in the region where the Irminger and East Greenland Currents act. Therefore, nutrient-enriched waters must have been advected further north into the Labrador Sea to regions with favorable conditions for phytoplankton growth by April-May. This nutrient enrichment in turn enhanced phytoplankton growth along the coast of western Greenland, and possibly further offshore through eddy transport (Chanut et al. 2008; Frajka-Williams and Rhines 2010).

Further indication of a strong advective signal can be implied by patches of extremely high chlorophyll-a concentrations in May distributions during years of enhanced Labrador Sea productivity (e.g., 2014, 2015). One can observe patches of up to 30-50 $\mathrm{mg\,m^{-3}}$ (Figure 3), which cannot be attributed solely to in-situ growth. These levels are 2- to 4-fold above the available winter nitrate concentrations of $\sim$15 $\mathrm{\mu mol\,kg^{-1}}$ (Figure 8), which would allow maximum chlorophyll-a concen-

tration of around 15 mg m^{-3} locally. With a polar diatom Si:N ratio of ~1.5 (Lomas et al. 2019), local concentrations due to silicate availability would be even more constrained. An accumulation mechanism is therefore indicated, one that leads to convergence of phytoplankton biomass in the bloom region. Given that peak chlorophyll-a occurs in regions where enhanced eddy-kinetic energy occurs, similar transport mechanisms for nutrients from the Greenland shelf can be anticipated.

A comparison between satellite-based estimates of ~~phytoplankton biomass and productivity~~ chlorophyll-a concentrations and NPP with estimates from ocean models (Figure 1 and 5) makes clear that the available subset of models do not reproduce the variability in ~~Labrador Sea chlorophyll-a concentrations~~ phytoplankton communities of the Labrador Sea that is evident from satellite observations (Figure 1 and 5). This discrepancy indicates that the models do not adequately represent the connection between numerous physical processes and phytoplankton growth in this region. Model inadequacy in this regard is not unexpected, given that the North Atlantic is characterized by multiple distinct regions, each with its own dominant physical mechanisms and pattern of biological productivity.

Recent studies suggest that the melting of the Greenland ice sheet may influence phytoplankton blooms in the Labrador Sea, through two possible mechanisms. One is through an elevated supply of dissolved nutrients from glacial meltwater, and the other is through the impact of meltwater on surface stratification. The amount of meltwater discharged from Greenland ice melting has increased over the recent decades (Rignot et al. 2008; Bamber et al. 2012; Dukhovskoy et al. 2019), with striking summer melting in 2012 (Nghiem et al. 2012; Tedesco et al. 2013; Hanna et al. 2014). This melting is projected to double by the end of the twenty-first century (Fettweis et al. 2013). Through its impact on stratification and a reduction in light limitation conferred by shallower MLDs, Oliver et al. (2018) propose that stronger phytoplankton blooms will start to occur later in summer and fall, leading to increased primary productivity in the Labrador Sea.

Furthermore, the Greenland ice sheet is a potential source of bioavailable nutrients such as phosphorus (Hawkings et al. 2016), iron (Bhatia et al. 2013; Hawkings et al. 2014; Arrigo et al. 2017) and silicate (Meire et al. 2016). Hawkings et al. (2016) measured concentrations of reactive phosphorus in two glaciers that reached up to 0.35 μM. Dissolved iron concentrations were found to be on the order of 1-10μM, with particulate iron an order of magnitude higher (Bhatia et al. 2013). Silicate concentrations up to 15-30μM were measured in two fjords in northeast and southwest Greenland that are fed by land and marine-terminating glaciers (Meire et al. 2016). Besides the nutrient flux from the glacial meltwater itself, discharge of glacial melting from marine-terminating glaciers play an important role as it leads to upwelling of deep nutrient rich water (Hopwood et al. 2018; Cape et al. 2018).

Arrigo et al. (2017) suggested that discharge of meltwater from the Greenland ice sheet is associated with large-scale summer blooms in the Labrador Sea, accounting for about 40% of annual primary production, at distances of up to 300 km from the coast. Since this was not accompanied by a significant change in MLD, they reasoned that increased nutrient supply may be the determining factor in associating glacial meltwater with phytoplankton blooms. In particular, they cite evidence that macronutrient concentrations are not growth-rate limiting, and so conclude that enhanced iron supply from meltwater is the main driver of the large-scale summer blooms. In contrast, Meire et al. (2016) found that the export of dissolved silica in glacial meltwater is disproportionately high (i.e., up to 30 μM) relative to other macronutrients in two fjord systems adjacent to the Greenland ice sheet, and that the resulting increased Si:P ratio at the ocean surface is proposed to favor diatom growth above other types of phytoplankton.

It is not clear how far into the Labrador Sea the relevant area of impact of ice sheet meltwater reaches, or whether it is mainly constrained to the vicinity of the Greenland fjords. Luo et al. (2016) found that up to 60% of meltwater from southeast Greenland moves westwards into the northern

Labrador Sea by fall and early winter, which would affect stratification and nutrient concentrations far from the coast. Arrigo et al. (2017) also suggested that timing of the summer blooms during their study period is highly suggestive of a direct association with Greenland ice sheet melting. Given these time constraints, Greenland ice sheet meltwater would affect ocean productivity in the late summer and fall of the same year, and would likely not contribute to the nutrient pool in the following years. One indication that the high silicate values observed in the AR7W transect are not predominantly a result of Greenland ice sheet melting is that the year 2012, which was one of record ice sheet melting, did not lead to elevated silicate values in the following years (Figure 12). Furthermore, 2012 was a year with fairly low annual mean chlorophyll-a concentrations, calling into question the effect of Greenland ice sheet melting on summer production. A direct link between high silicate concentrations and Greenland ice sheet melting therefore cannot be established. One might assume a possible delay of 2-3 years, but this is not based on the estimated time it would take for this meltwater to reach the interior of Labrador Sea (Luo et al. 2016).

The above discussion gives fresh context to previous findings that spring bloom onset and intensity in the northern Labrador Sea is correlated with low-salinity water along the Greenland coast (Wu et al. 2008; Frajka-Williams et al. 2009; Frajka-Williams and Rhines 2010). Wu et al. (2008) found that the early onset of the spring bloom in the northern Labrador Sea is related to a reduced MLD associated with low-salinity water along the Greenland coast, although their work was focused on the factors that drive annual timing of the spring bloom, rather than long-term impacts on bloom magnitudes. Frajka-Williams et al. (2009) suggest that meltwater may increase boundary gradients in the West Greenland Current, potentially accelerating the SPG which would in turn lead to an increase in eddy production. However, they did not find any significant correlations between meltwater runoff and offshore velocity or eddy kinetic energy. However, Frajka-Williams and Rhines (2010) did find that the intensity of the bloom in the northern Labrador Sea correlated

with offshore advection, eddy activity, and runoff from Greenland on interannual time scales. This is consistent with our findings that associate a stronger SPG with an increase in nutrient flux along the West Greenland Current and more intense spring blooms in the Labrador Sea. However, we identify the underlying mechanism for this increase in spring blooms to be the vertical supply of nutrients through winter convection, the recent enhancement of which likely fueled the intense spring blooms and strengthened the SPG.

5. Conclusion

Here a recent nutrient enrichment in the intermediate Labrador Sea has been documented, attributed to enhanced winter convection and used to explain the observations of higher annual mean chlorophyll-a concentrations in the Labrador Sea. The positive correlation of nutrients and convection depth in the upper 1000 m of the Labrador Sea (Figure 18) indicates that during winters with anomalously deep convection, entrainment of nutrient-rich waters prevails over mixing of depleted waters, and conversely in winters in which convection depth is shallower than usual a net loss of nutrients moving into the deeper ocean (particularly silicate) can be expected. There is also a correlation between silicate concentration and the strength of the SPG, which is explained by the strong correlation between the subpolar gyre index and convection depth (Figure 15). Even though a causal link between gyre strength and nutrient concentrations can not be ruled out, the correlation patterns between nutrients and convection depth suggest a dominant role of vertical redistribution in regulating nutrient availability in the Labrador Sea.

Deeper winter convective mixing drives vertical nutrient supply which in turn is associated with higher annual mean chlorophyll-a in the Labrador Sea (as observed from satellite). In particular, stronger winter convection affects the nutrient upwelling in the vicinity of the West Greenland and Irminger Current, where water flows northwest along Greenland. This potentially leads to

more nutrients reaching the northern Labrador Sea fueling the spring blooms observed in this area (Figure 3). Mean concentrations do not suggest silicate limitation during the time of the cruise. However, it could very well be that nutrient limitation will occur later in the summer. Thus, the correlations between silicate and annual mean chlorophyll-a concentration can be explained by enduring nutrient supply throughout the growing season. Conversely, chlorophyll-a trends are negative in the eastern SPNA (i.e., between Iceland and Scotland; Figure 1), indicating that other factors are acting in this region and that the link between nutrient enrichment and chlorophyll-a concentration is constrained to the Labrador Sea. It should be noted though that the additional nutrients now enriching the Labrador Sea may eventually be advected into the eastern SPNA, such that this region may at some point in the future also experience increased productivity.

The Labrador Sea is a crucial source for the redistribution of nutrients to the western North Atlantic, through deep mixing and horizontal circulation. In particular, the Labrador Current has been identified as an important conveyor of nutrients into the North Atlantic (Torres-Valdes et al. 2013). Therefore, variation in nutrient concentrations in the upper Labrador Sea has important implications for nutrient availability over the entire North Atlantic. A centennial decline in the Atlantic Meridional Overturning Circulation (AMOC) has been identified as a driver of long term reduction in ocean productivity over the subpolar North Atlantic (Osman et al. 2019). The idea confirms prior modeling analysis (e.g., Schmittner 2005) predicting that a decline in the AMOC strength would reduce globally integrated export production. The AMOC is connected to Labrador Sea Water formation. The present study has shown the effect of deep water formation on nutrient levels in the upper Labrador Sea, and connects this to recent variability in ~~phytoplankton biomass~~chlorophyll-a concentrations, thereby providing a direct link between changes in the AMOC and ~~variability in phytoplankton biomass and ocean productivity~~the Labrador Sea ecosystem.

Acknowledgments. JET acknowledges funding from NASA's Goddard Space Flight Center (award number NNX15AN27H). We thank the many people and projects that made this work possible through the free availability of ocean data~~is gratefully acknowledged~~. These include the International Argo Program and the national programs that contribute to it as part of the Global Ocean Observing System (`http://www.argo.ucsd.edu`, `http://argo.jcommops.org`)~~;~~ ~~Bedford Institute of Oceanography (BIO) and the Atlantic Zone Off-Shelf Monitoring Program (AZOMP, ; ~~. We made use of shipboard datasets provided by the Global Ocean Data Analysis Project version 2 (GLODAPv2 (`https://www.nodc.noaa.gov/ocads/oceans/GLODAPv2_2019/`)~~; the NASA Ocean Color data center (GSFC,), Ocean Productivity Group, Oregon State University (), ~~, the Bedford Institute of Oceanography (BIO), and the Deep-Ocean Observation and Research Synthesis (DOORS) project initiated and led by IY at BIO as a follow-up of the World Ocean Circulation Experiment (WOCE). Satellite data of chlorophyll-a were obtained from the NASA Ocean Color data center (GSFC, `https://oceancolor.gsfc.nasa.gov`). Monthly fields of chlorophyll-a and NPP were retrieved from the Ocean Productivity Group, Oregon State University (`http://sites.science.oregonstate.edu/ocean.productivity`). Thank you to Greg Silsbe for providing monthly NPP fields derived from CAFE. Surface drifter data were obtained from processed delayed mode hourly data (`https://www.aoml.noaa.gov/phod/gdp/hourly_data.php`) and real-time variable-time-step data (`https://www.aoml.noaa.gov/phod/gdp/real-time_data.php`). This study benefited from discussions with Ryan Abernathey, Stephen Griffies, John Krasting, Galen McKinley and Graeme MacGilchrist. We also thank the editor and two anonymous reviewers for their careful assessment and suggestions to improve the manuscript.

References

Aksnesa, D. L., and M. D. Ohman, 2009: Multi-decadal shoaling of the euphotic zone in the southern sector of the California Current System. *Limnology and Oceanography*, **54 (4)**, 1272–1281, doi:10.4319/lo.2009.54.4.1272.

Armbrust, E. V., 2009: The life of diatoms in the world's oceans. *Nature*, **459 (7244)**, 185 – 192, doi:10.1038/nature08057.

Arrigo, K. R., and Coauthors, 2017: Melting glaciers stimulate large summer phytoplankton blooms in southwest Greenland waters. *Geophysical Research Letters*, **44 (12)**, 6278–6285, doi:10.1002/2017GL073583.

Aumont, O., C. Ethé, A. Tagliabue, L. Bopp, and M. Gehlen, 2015: PISCES-v2: an ocean biogeochemical model for carbon and ecosystem studies. *Geoscientific Model Development*, **8 (8)**, 2465–2513, doi:10.5194/gmd-8-2465-2015, URL https://www.geosci-model-dev.net/8/2465/2015/.

Balaguru, K., S. C. Doney, L. Bianucci, P. J. Rasch, L. R. Leung, J.-H. Yoon, and I. D. Lima, 2018: Linking deep convection and phytoplankton blooms in the northern Labrador Sea in a changing climate. *PLOS ONE*, **13 (1)**, 1–17, doi:10.1371/journal.pone.0191509, URL https://doi.org/10.1371/journal.pone.0191509.

Bamber, J., M. van den Broeke, J. Ettema, J. Lenaerts, and E. Rignot, 2012: Recent large increases in freshwater fluxes from Greenland into the North Atlantic. *Geophysical Research Letters*, **39 (19)**, doi:10.1029/2012GL052552, URL https://agupubs.onlinelibrary.wiley.com/doi/abs/10.1029/2012GL052552, https://agupubs.onlinelibrary.wiley.com/doi/pdf/10.1029/2012GL052552.

962 Barton, A. D., M. S. Lozier, and R. G. Williams, 2014: Physical controls of variability in North
963 Atlantic phytoplankton communities. *Limnology and Oceanography*, **60 (1)**, 181–197, doi:
964 10.1002/lno.10011, URL https://aslopubs.onlinelibrary.wiley.com/doi/abs/10.1002/lno.10011,
965 https://aslopubs.onlinelibrary.wiley.com/doi/pdf/10.1002/lno.10011.

966 Beaulieu, C., S. A. Henson, J. L. Sarmiento, J. P. Dunne, S. C. Doney, R. R. Rykaczewski, and
967 L. Bopp, 2013: Factors challenging our ability to detect long-term trends in ocean chlorophyll.
968 *Biogeosciences*, **10 (4)**, 2711–2724, doi:10.5194/bg-10-2711-2013.

969 Behrenfeld, M. J., 2010: Abandoning Sverdrup's Critical Depth Hypothesis on phytoplankton
970 blooms. *Ecology*, **91 (4)**, 977–989, doi:10.1890/09-1207.1, URL https://esajournals.onlinelibrary.
971 wiley.com/doi/abs/10.1890/09-1207.1, https://esajournals.onlinelibrary.wiley.com/doi/pdf/10.
972 1890/09-1207.1.

973 Behrenfeld, M. J., E. Boss, D. A. Siegel, and D. M. Shea, 2005: Carbon-based ocean productivity
974 and phytoplankton physiology from space. *Global Biogeochemical Cycles*, **19 (1)**, doi:10.1029/
975 2004GB002299, URL https://agupubs.onlinelibrary.wiley.com/doi/abs/10.1029/2004GB002299,
976 https://agupubs.onlinelibrary.wiley.com/doi/pdf/10.1029/2004GB002299.

977 Behrenfeld, M. J., and E. S. Boss, 2017: Student's tutorial on bloom hypotheses in the context of
978 phytoplankton annual cycles. *Global Change Biology*, **24 (1)**, 55–77, doi:10.1111/gcb.13858,
979 URL https://onlinelibrary.wiley.com/doi/abs/10.1111/gcb.13858, https://onlinelibrary.wiley.com/
980 doi/pdf/10.1111/gcb.13858.

981 Behrenfeld, M. J., S. C. Doney, I. Lima, E. S. Boss, and D. A. Siegel, 2013: Annual cycles of
982 ecological disturbance and recovery underlying the subarctic Atlantic spring plankton bloom.
983 *Global Biogeochemical Cycles*, **27 (2)**, 526–540, doi:10.1002/gbc.20050, URL https://agupubs.

onlinelibrary.wiley.com/doi/abs/10.1002/gbc.20050, https://agupubs.onlinelibrary.wiley.com/doi/pdf/10.1002/gbc.20050.

Behrenfeld, M. J., and P. G. Falkowski, 1997: Photosynthetic rates derived from satellite-based chlorophyll concentration. *Limnology and Oceanography*, **42 (1)**, 1–20, doi:10.4319/lo.1997.42.1.0001, URL https://aslopubs.onlinelibrary.wiley.com/doi/abs/10.4319/lo.1997.42.1.0001, https://aslopubs.onlinelibrary.wiley.com/doi/pdf/10.4319/lo.1997.42.1.0001.

Behrenfeld, M. J., and Coauthors, 2006: Climate-driven trends in contemporary ocean productivity. *Nature*, **444 (7120)**, 752–755, doi:10.1038/nature05317, URL https://www.nature.com/articles/nature05317.

Bennington, V., G. A. McKinley, S. Dutkiewicz, and D. Ullman, 2009: What does chlorophyll variability tell us about export and air-sea CO2 flux variability in the North Atlantic? *Global Biogeochemical Cycles*, **23 (3)**, doi:10.1029/2008GB003241, URL https://agupubs.onlinelibrary.wiley.com/doi/abs/10.1029/2008GB003241, https://agupubs.onlinelibrary.wiley.com/doi/pdf/10.1029/2008GB003241.

Bhatia, M. P., E. B. Kujawinski, S. B. Das, C. F. Breier, P. B. Henderson, and M. A. Charette, 2013: Greenland meltwater as a significant and potentially bioavailable source of iron to the ocean. *Nature Geoscience*, **6 (4)**, 274–278, doi:10.1038/ngeo1746.

Boss, E., and M. Behrenfeld, 2010: In situ evaluation of the initiation of the North Atlantic phytoplankton bloom. *Geophysical Research Letters*, **37 (18)**, doi:10.1029/2010GL044174, URL https://agupubs.onlinelibrary.wiley.com/doi/abs/10.1029/2010GL044174, https://agupubs.onlinelibrary.wiley.com/doi/pdf/10.1029/2010GL044174.

Brody, S. R., and M. S. Lozier, 2015: Characterizing upper-ocean mixing and its effect on the spring phytoplankton bloom with in situ data. *ICES Journal of Marine Science*, **72 (6)**, 1961–1970, doi:10.1093/icesjms/fsv006.

Bryden, H. L., W. E. Johns, B. A. King, G. McCarthy, E. L. McDonagh, B. I. Moat, and D. A. Smeed, 2020: Reduction in Ocean Heat Transport at 26°N since 2008 Cools the Eastern Subpolar Gyre of the North Atlantic Ocean. *Journal of Climate*, **33 (5)**, 1677–1689, doi:10.1175/JCLI-D-19-0323.1.

Brzezinski, M. A., 1985: The Si:C:N ratio of marine diatoms: interspecific variability and the effect of some environmental variables. *Journal of Phycology*, **21 (3)**, 347–357, doi:10.1111/j.0022-3646.1985.00347.x.

Brzezinski, M. A., and Coauthors, 2002: A switch from $Si(OH)_4$ to NO_3^- depletion in the glacial Southern Ocean. *Geophysical Research Letters*, **29 (1)**, 1564, doi:10.1029/2001GL014349.

Cape, M. R., F. Straneo, N. Beaird, R. M. Bundy, and M. A. Charette, 2018: Nutrient release to oceans from buoyancy-driven upwelling at Greenland tidewater glaciers. *Nature Geoscience*, **12 (1)**, 1–8, doi:10.1038/s41561-018-0268-4.

Chanut, J., B. Barnier, W. Large, L. Debreu, T. Penduff, J.-M. Molines, and P. Mathiot, 2008: Mesoscale Eddies in the Labrador Sea and Their Contribution to Convection and Restratification. *Journal of Physical Oceanography*, **38 (8)**, 1617–1643, doi:10.1175/2008JPO3485.1.

Comiso, J. C., C. L. Parkinson, R. Gersten, and L. Stock, 2008: Accelerated decline in the Arctic sea ice cover. *Geophysical Research Letters*, **35 (1)**, doi:10.1029/2007GL031972.

Curry, R., B. Dickson, and I. Yashayaev, 2003: A change in the freshwater balance of the Atlantic Ocean over the past four decades. *Nature*, **426 (6968)**, 826–829, doi:10.1038/nature02206.

Dickson, B., I. Yashayaev, J. Meincke, B. Turrell, S. R. Dye, and J. Holfort, 2002: Rapid freshening of the deep North Atlantic Ocean over the past four decades. *Nature*, **416 (6883)**, 832–837.

Doney, S. C., 2006: Plankton in a warmer world. *Nature*, **444**, 695–696, doi:10.1038/444695a, URL https://www.nature.com/articles/444695a.

Duchez, A., and Coauthors, 2016: Drivers of exceptionally cold North Atlantic Ocean temperatures and their link to the 2015 European heat wave. *Environmental Research Letters*, **11 (7)**, 074 004, doi:10.1088/1748-9326/11/7/074004.

Dukhovskoy, D. S., I. Yashayaev, A. Proshutinsky, J. L. Bamber, I. L. Bashmachnikov, E. P. Chassignet, C. M. Lee, and A. J. Tedstone, 2019: Role of Greenland Freshwater Anomaly in the Recent Freshening of the Subpolar North Atlantic. *Journal of Geophysical Research: Oceans*, **124 (5)**, 3333–3360, doi:10.1029/2018JC014686.

Durack, P. J., S. E. Wijffels, and R. J. Matear, 2012: Ocean salinities reveal strong global water cycle intensification during 1950 to 2000. *Science*, **336 (6080)**, 455–458, doi:10.1126/science.1212222.

Egge, J. K., and D. L. Aksnes, 1992: Silicate as regulating nutrient in phytoplankton competition. *Marine Ecology Progress Series*, **83**, 281–289, doi:10.3354/meps083281.

Fay, A. R., and G. A. McKinley, 2017: Correlations of surface ocean pCO2 to satellite chlorophyll on monthly to interannual timescales. *Global Biogeochemical Cycles*, **31 (3)**, 436–455, doi:10.1002/2016GB005563, URL https://agupubs.onlinelibrary.wiley.com/doi/abs/10.1002/2016GB005563, https://agupubs.onlinelibrary.wiley.com/doi/pdf/10.1002/2016GB005563.

Fettweis, X., B. Franco, M. Tedesco, J. H. van Angelen, J. T. M. Lenaerts, M. R. van den Broeke, and H. Gallée, 2013: Estimating the Greenland ice sheet surface mass balance contribution to

future sea level rise using the regional atmospheric climate model MAR. *The Cryosphere*, **7 (2)**, 469–489, doi:10.5194/tc-7-469-2013, URL https://www.the-cryosphere.net/7/469/2013/.

Foukal, N. P., and M. S. Lozier, 2017: Assessing variability in the size and strength of the North Atlantic subpolar gyre. *Journal of Geophysical Research: Oceans*, **122 (8)**, 6295–6308, doi:10.1002/2017JC012798, URL https://agupubs.onlinelibrary.wiley.com/doi/abs/10.1002/2017JC012798, https://agupubs.onlinelibrary.wiley.com/doi/pdf/10.1002/2017JC012798.

Fragoso, G. M., A. J. Poulton, I. M. Yashayaev, E. J. H. Head, G. Johnsen, and D. A. Purdie, 2018: Diatom biogeography from the Labrador Sea revealed through a trait-based approach. *Frontiers in Marine Science*, **5**, doi:10.3389/fmars.2018.00297.

Fragoso, G. M., A. J. Poulton, I. M. Yashayaev, E. J. H. Head, and D. A. Purdie, 2017: Spring phytoplankton communities of the Labrador Sea (2005–2014): pigment signatures, photophysiology and elemental ratios. *Biogeosciences*, **14 (5)**, 1235–1259, doi:10.5194/bg-14-1235-2017.

Fragoso, G. M., A. J. Poulton, I. M. Yashayaev, E. J. H. Head, M. C. Stinchcombe, and D. A. Purdie, 2016: Biogeographical patterns and environmental controls of phytoplankton communities from contrasting hydrographical zones of the Labrador Sea. *Progress in Oceanography*, **141 (C)**, 212–226, doi:10.1016/j.pocean.2015.12.007.

Frajka-Williams, E., and P. B. Rhines, 2010: Physical controls and interannual variability of the Labrador Sea spring phytoplankton bloom in distinct regions. *Deep Sea Research Part I: Oceanographic Research Papers*, **57 (4)**, 541–552, doi:10.1016/j.dsr.2010.01.003, URL http://www.sciencedirect.com/science/article/pii/S0967063710000270.

Frajka-Williams, E., P. B. Rhines, and C. C. Eriksen, 2009: Physical controls and mesoscale variability in the Labrador Sea spring phytoplankton bloom observed by Seaglider. *Deep Sea*

Research Part I: Oceanographic Research Papers, **56 (12)**, 2144–2161, doi:10.1016/j.dsr.2009.07.008, URL http://www.sciencedirect.com/science/article/pii/S0967063709001642.

Garcia, H. E., and Coauthors, 2019: World Ocean Atlas 2018. Vol. 4: Dissolved Inorganic Nutrients (phosphate, nitrate and nitrate+nitrite, silicate). A. Mishonov Technical Editor, NOAA Atlas NESDIS 84, 35pp.

Gaube, P., D. J. McGillicuddy Jr., and A. J. Moulin, 2019: Mesoscale Eddies Modulate Mixed Layer Depth Globally. *Geophysical Research Letters*, **46 (3)**, 1505–1512, doi:10.1029/2018gl080006.

Glover, D. M., and P. G. Brewer, 1988: Estimates of wintertime mixed layer nutrient concentrations in the North Atlantic. *Deep Sea Research Part A*, **35 (9)**, 1525–1546, doi:10.1016/0198-0149(88)90101-X.

Gregg, W. W., and N. W. Casey, 2007: Modeling coccolithophores in the global oceans. *Deep Sea Research Part II: Topical Studies in Oceanography*, **54 (5)**, 447–477, doi:10.1016/j.dsr2.2006.12.007, URL http://www.sciencedirect.com/science/article/pii/S0967064507000318, the Role of Marine Organic Carbon and Calcite Fluxes in Driving Global Climate Change, Past and Future.

Gregg, W. W., and C. S. Rousseaux, 2014: Decadal trends in global pelagic ocean chlorophyll: A new assessment integrating multiple satellites, in situ data, and models. *Journal of Geophysical Research: Oceans*, **119 (9)**, 5921 – 5933, doi:10.1002/2014jc010158.

Grist, J. P., S. A. Josey, Z. L. Jacobs, R. Marsh, B. Sinha, and E. Sebille, 2016: Extreme air–sea interaction over the North Atlantic subpolar gyre during the winter of 2013–2014 and its subsurface legacy. *Climate Dynamics*, **46 (11)**, 4027–4045, doi:10.1007/s00382-015-2819-3.

Häkkinen, S., and P. B. Rhines, 2004: Decline of Subpolar North Atlantic Circulation During the 1990s. *Science*, **304 (5670)**, 555–559, doi:10.1126/science.1094917, URL https://science.

sciencemag.org/content/304/5670/555, https://science.sciencemag.org/content/304/5670/555.full.pdf.

Hanna, E., and Coauthors, 2014: Atmospheric and oceanic climate forcing of the exceptional Greenland ice sheet surface melt in summer 2012. *International Journal of Climatology*, **34 (4)**, 1022–1037, doi:10.1002/joc.3743, URL https://rmets.onlinelibrary.wiley.com/doi/abs/10.1002/joc.3743, https://rmets.onlinelibrary.wiley.com/doi/pdf/10.1002/joc.3743.

Harrison, W. G., K. Y. Børsheim, W. K. Li, G. L. Maillet, P. Pepin, E. Sakshaug, M. D. Skogen, and P. A. Yeats, 2013: Phytoplankton production and growth regulation in the Subarctic North Atlantic: A comparative study of the Labrador Sea-Labrador/Newfoundland shelves and Barents/Norwegian/Greenland seas and shelves. *Progress in Oceanography*, **114**, 26–45, doi:10.1016/j.pocean.2013.05.003, URL http://www.sciencedirect.com/science/article/pii/S0079661113000451, norway-Canada Comparison of Marine Ecosystems (NORCAN).

Hátún, H., A. B. Sandø, H. Drange, B. Hansen, and H. Valdimarsson, 2005: Influence of the Atlantic Subpolar Gyre on the Thermohaline Circulation. *Science*, **309 (5742)**, 1841–1844, doi:10.1126/science.1114777, URL https://science.sciencemag.org/content/309/5742/1841, https://science.sciencemag.org/content/309/5742/1841.full.pdf.

Hátún, H., and Coauthors, 2016: An inflated subpolar gyre blows life toward the northeastern Atlantic. *Progress in Oceanography*, **147**, 49–66, doi:10.1016/j.pocean.2016.07.009, URL http://www.sciencedirect.com/science/article/pii/S007966111630129X.

Hátún, H., and Coauthors, 2017: The subpolar gyre regulates silicate concentrations in the North Atlantic. *Scientific Reports*, **7 (1)**, 14 576, doi:10.1038/s41598-017-14837-4.

Hawkings, J., and Coauthors, 2016: The Greenland Ice Sheet as a hot spot of phosphorus weathering and export in the Arctic. *Global Biogeochemical Cycles*, **30 (2)**, 191–210, doi: 10.1002/2015GB005237.

Hawkings, J. R., and Coauthors, 2014: Ice sheets as a significant source of highly reactive nanoparticulate iron to the oceans. *Nature Communications*, **5**, 3929, doi:10.1038/ncomms4929.

Henson, S. A., 2014: Slow science: the value of long ocean biogeochemistry records. *Philosophical Transactions of the Royal Society A: Mathematical, Physical and Engineering Sciences*, **372 (2025)**, doi:10.1098/rsta.2013.0334.

Henson, S. A., S. C. Painter, N. Penny Holliday, M. C. Stinchcombe, and S. L. C. Giering, 2013: Unusual subpolar North Atlantic phytoplankton bloom in 2010: Volcanic fertilization or North Atlantic Oscillation? *Journal of Geophysical Research: Oceans*, **118 (10)**, 4771–4780, doi:10.1002/jgrc.20363.

Holliday, N. P., and Coauthors, 2020: Ocean circulation causes the largest freshening event for 120 years in eastern subpolar North Atlantic. *Nature Communications*, **11 (1)**, 1–15, doi: 10.1038/s41467-020-14474-y.

Holte, J., and L. Talley, 2009: A New Algorithm for Finding Mixed Layer Depths with Applications to Argo Data and Subantarctic Mode Water Formation. *Journal of Atmospheric and Oceanic Technology*, **26 (9)**, 1920–1939, doi:10.1175/2009JTECHO543.1.

Holte, J., L. D. Talley, J. Gilson, and D. Roemmich, 2017: An Argo mixed layer climatology and database. *Geophysical Research Letters*, **44 (11)**, 5618–5626, doi:10.1002/2017GL073426.

Hopwood, M. J., D. Carroll, T. J. Browning, L. Meire, J. Mortensen, S. Krisch, and E. P. Achterberg, 2018: Non-linear response of summertime marine productivity to increased meltwater discharge around Greenland. *Nature Communications*, **9 (1)**, 1–9, doi:10.1038/s41467-018-05488-8.

Hopwood, M. J., and Coauthors, 2019: Highly variable iron content modulates iceberg- ocean fertilisation and potential carbon export. *Nature Communications*, **10 (1)**, 1–10, doi:10.1038/s41467-019-13231-0.

Körtzinger, A., U. Send, D. W. R. Wallace, J. Karstensen, and M. DeGrandpre, 2008: Seasonal cycle of O2 and pCO2 in the central Labrador Sea: Atmospheric, biological, and physical implications. *Global Biogeochemical Cycles*, **22 (1)**, doi:10.1029/2007GB003029.

Koul, V., and Coauthors, 2020: Unraveling the choice of the north Atlantic subpolar gyre index. *Scientific Reports*, **10 (1)**, 1005–12, doi:10.1038/s41598-020-57790-5.

Krause, J. W., I. K. Schulz, K. A. Rowe, W. Dobbins, M. H. S. Winding, M. K. Sejr, C. M. Duarte, and S. Agustí, 2019: Silicic acid limitation drives bloom termination and potential carbon sequestration in an Arctic bloom. *Scientific Reports*, **9 (1)**, 8149, doi:10.1038/s41598-019-44587-4.

Lacour, L., H. Claustre, L. Prieur, and F. D'Ortenzio, 2015: Phytoplankton biomass cycles in the North Atlantic subpolar gyre: A similar mechanism for two different blooms in the Labrador Sea. *Geophysical Research Letters*, **42 (13)**, 5403–5410, doi:10.1002/2015GL064540.

Lomas, M. W., S. E. Baer, S. Acton, and J. W. Krause, 2019: Pumped Up by the Cold: Elemental Quotas and Stoichiometry of Cold-Water Diatoms. *Frontiers in Marine Science*, **6**, 170, doi:10.3389/fmars.2019.00286.

Luo, H., R. M. Castelao, A. K. Rennermalm, M. Tedesco, A. Bracco, P. L. Yager, and T. L. Mote, 2016: Oceanic transport of surface meltwater from the southern Greenland ice sheet.

Nature Geoscience, **9**, 528–532, doi:10.1038/ngeo2708, URL https://www.nature.com/articles/ngeo2708.

Marchese, C., L. C. de la Guardia, P. G. Myers, and S. Bélanger, 2019: Regional differences and inter-annual variability in the timing of surface phytoplankton blooms in the Labrador Sea. *Ecological Indicators*, **96 (Part 1)**, 81–90, doi:10.1016/j.ecolind.2018.08.053.

Martinez, E., D. Antoine, F. D'Ortenzio, and B. Gentili, 2009: Climate-Driven Basin-Scale Decadal Oscillations of Oceanic Phytoplankton. *Science*, **326 (5957)**, 1253–1256, doi:10.1126/science.1177012.

Martinez, E., D. E. Raitsos, and D. Antoine, 2016: Warmer, deeper, and greener mixed layers in the North Atlantic subpolar gyre over the last 50 years. *Global Change Biology*, **22 (2)**, 604–612, doi:10.1111/gcb.13100, URL https://onlinelibrary.wiley.com/doi/abs/10.1111/gcb.13100, https://onlinelibrary.wiley.com/doi/pdf/10.1111/gcb.13100.

McKinley, G. A., A. L. Ritzer, and N. S. Lovenduski, 2018: Mechanisms of northern North Atlantic biomass variability. *Biogeosciences*, **15 (20)**, 6049–6066, doi:10.5194/bg-15-6049-2018.

Meire, L., and Coauthors, 2016: High export of dissolved silica from the Greenland Ice Sheet. *Geophysical Research Letters*, **43 (17)**, 9173–9182, doi:10.1002/2016GL070191.

Nghiem, S. V., and Coauthors, 2012: The extreme melt across the Greenland ice sheet in 2012. *Geophysical Research Letters*, **39 (20)**, doi:10.1029/2012GL053611.

Oliver, H., and Coauthors, 2018: Exploring the Potential Impact of Greenland Meltwater on Stratification, Photosynthetically Active Radiation, and Primary Production in the Labrador Sea. *Journal of Geophysical Research: Oceans*, **123 (4)**, 2570–2591, doi:10.1002/2018JC013802.

1176 Olsen, A., and Coauthors, 2016: The Global Ocean Data Analysis Project version 2 (GLODAPv2)
1177 – an internally consistent data product for the world ocean. *Earth System Science Data*, **8 (2)**,
1178 297–323, doi:10.5194/essd-8-297-2016, URL https://www.earth-syst-sci-data.net/8/297/2016/.

1179 Osman, M. B., and Coauthors, 2019: Industrial-era decline in subarctic Atlantic productivity.
1180 *Nature*, **569 (7757)**, 1–22, doi:10.1038/s41586-019-1181-8.

1181 Parkinson, C. L., and J. C. Comiso, 2013: On the 2012 record low Arctic sea ice cover: Combined
1182 impact of preconditioning and an August storm. *Geophysical Research Letters*, **40 (7)**, 1356–
1183 1361, doi:10.1002/grl.50349.

1184 Piecuch, C. G., R. M. Ponte, C. M. Little, M. W. Buckley, and I. Fukumori, 2017: Mechanisms
1185 underlying recent decadal changes in subpolar North Atlantic Ocean heat content. *Journal of*
1186 *Geophysical Research: Oceans*, **122 (9)**, 7181–7197, doi:10.1002/2017JC012845.

1187 Polovina, J. J., E. A. Howell, and M. Abecassis, 2008: Ocean's least productive waters are
1188 expanding. *Geophysical Research Letters*, **35 (3)**, doi:10.1029/2007GL031745.

1189 Ragueneau, O., and Coauthors, 2000: A review of the Si cycle in the modern ocean: recent progress
1190 and missing gaps in the application of biogenic opal as a paleoproductivity proxy. *Global and*
1191 *Planetary Change*, **26 (4)**, 317–365, doi:10.1016/S0921-8181(00)00052-7.

1192 Rahmstorf, S., J. E. Box, G. Feulner, M. E. Mann, A. Robinson, S. Rutherford, and E. J. Schaffer-
1193 nicht, 2015: Exceptional twentieth-century slowdown in Atlantic Ocean overturning circulation.
1194 *Nature Climate Change*, **5 (5)**, 475–480, doi:10.1126/science.aaa4019.

1195 Rhein, M., R. Steinfeldt, D. Kieke, I. Stendardo, and I. Yashayaev, 2017: Ventilation variability
1196 of Labrador Sea Water and its impact on oxygen and anthropogenic carbon: a review. *Philo-*

sophical Transactions of the Royal Society A: Mathematical, Physical and Engineering Sciences, **375 (2102)**, 20160 321, doi:10.1098/rsta.2016.0321.

Rignot, E., J. E. Box, E. Burgess, and E. Hanna, 2008: Mass balance of the Greenland ice sheet from 1958 to 2007. *Geophysical Research Letters*, **35 (20)**, doi:10.1029/2008GL035417, URL https://agupubs.onlinelibrary.wiley.com/doi/abs/10.1029/2008GL035417, https://agupubs.onlinelibrary.wiley.com/doi/pdf/10.1029/2008GL035417.

Robson, J., P. Ortega, and R. Sutton, 2016: A reversal of climatic trends in the North Atlantic since 2005. *Nature Geoscience*, **9**, 513–517, doi:10.1038/ngeo2727.

Sarmiento, J. L., N. Gruber, M. A. Brzezinski, and J. P. Dunne, 2004: High-latitude controls of thermocline nutrients and low latitude biological productivity. *Nature*, **427 (6969)**, 56–60, doi:10.1038/nature02127.

Schmittner, A., 2005: Decline of the marine ecosystem caused by a reduction in the Atlantic overturning circulation. *Nature*, **434 (7033)**, 628–633, doi:10.1038/nature03476.

Siegel, D. A., S. C. Doney, and J. A. Yoder, 2002: The North Atlantic Spring Phytoplankton Bloom and Sverdrup's Critical Depth Hypothesis. *Science*, **296 (5568)**, 730–733, doi:10.1126/science.1069174.

Siegel, D. A., and Coauthors, 2013: Regional to global assessments of phytoplankton dynamics from the SeaWiFS mission. *Remote Sensing of Environment*, **135**, 77–91, doi:10.1016/j.rse.2013.03.025.

Silsbe, G. M., M. J. Behrenfeld, K. H. Halsey, A. J. Milligan, and T. K. Westberry, 2016: The CAFE model: A net production model for global ocean phytoplankton. *Global Biogeochemical Cycles*, **30 (12)**, 1756–1777, doi:10.1002/2016GB005521, URL https://agupubs.onlinelibrary.

wiley.com/doi/abs/10.1002/2016GB005521, https://agupubs.onlinelibrary.wiley.com/doi/pdf/10.1002/2016GB005521.

Skliris, N., R. Marsh, J. V. Mecking, and J. D. Zika, 2020: Changing water cycle and freshwater transports in the Atlantic Ocean in observations and CMIP5 models. *Climate Dynamics*, **31 (1)**, 1–19, doi:10.1007/s00382-020-05261-y.

Sverdrup, H. U., 1953: On Conditions for the Vernal Blooming of Phytoplankton. *ICES Journal of Marine Science*, **18 (3)**, 287–295, doi:10.1093/icesjms/18.3.287.

Tedesco, M., X. Fettweis, T. Mote, J. Wahr, P. Alexander, J. E. Box, and B. Wouters, 2013: Evidence and analysis of 2012 Greenland records from spaceborne observations, a regional climate model and reanalysis data. *The Cryosphere*, **7 (2)**, 615–630, doi:10.5194/tc-7-615-2013.

Tesdal, J., and T. W. N. Haine, 2020: Dominant Terms in the Freshwater and Heat Budgets of the Subpolar North Atlantic Ocean and Nordic Seas From 1992 to 2015. *Journal of Geophysical Research: Oceans*, **125 (10)**, doi:10.1029/2020jc016435.

Tesdal, J.-E., R. P. Abernathey, J. I. Goes, A. L. Gordon, and T. W. N. Haine, 2018: Salinity Trends within the Upper Layers of the Subpolar North Atlantic. *Journal of Climate*, **31 (7)**, 2675–2698, doi:10.1175/JCLI-D-17-0532.1.

Thomalla, S. J., A. J. Poulton, R. Sanders, R. Turnewitsch, P. M. Holligan, and M. I. Lucas, 2008: Variable export fluxes and efficiencies for calcite, opal, and organic carbon in the Atlantic Ocean: A ballast effect in action? *Global Biogeochemical Cycles*, **22 (1)**, doi:10.1029/2007GB002982.

Torres-Valdes, S., and Coauthors, 2013: Export of nutrients from the Arctic Ocean. *Journal of Geophysical Research: Oceans*, **118 (4)**, 1625–1644, doi:10.1002/jgrc.20063.

Tremblay, J., Y. Gratton, E. C. Carmack, C. D. Payne, and N. M. Price, 2002: Impact of the large-scale Arctic circulation and the North Water Polynya on nutrient inventories in Baffin Bay. *Journal of Geophysical Research: Oceans*, **107 (C8)**, doi:10.1029/2000jc000595.

Weeks, A. R., M. J. R. Fasham, J. Aiken, D. S. Harbour, J. F. Read, and I. Bellan, 1993: The spatial and temporal development of the spring bloom during the JGOFS North Atlantic Bloom Experiment, 1989. *Journal of the Marine Biological Association of the United Kingdom*, **73 (2)**, 253–282, doi:10.1017/s0025315400032847.

Westberry, T., M. J. Behrenfeld, D. A. Siegel, and E. Boss, 2008: Carbon-based primary productivity modeling with vertically resolved photoacclimation. *Global Biogeochemical Cycles*, **22 (2)**, doi:10.1029/2007GB003078, URL https://agupubs.onlinelibrary.wiley.com/doi/abs/10.1029/2007GB003078, https://agupubs.onlinelibrary.wiley.com/doi/pdf/10.1029/2007GB003078.

Westberry, T. K., P. Schultz, M. J. Behrenfeld, J. P. Dunne, M. R. Hiscock, S. Maritorena, J. L. Sarmiento, and D. A. Siegel, 2016: Annual cycles of phytoplankton biomass in the subarctic Atlantic and Pacific Ocean. *Global Biogeochemical Cycles*, **30 (2)**, 175–190, doi:10.1002/2015GB005276.

Wu, Y., T. Platt, C. C. L. Tang, and S. Sathyendranath, 2008: Regional differences in the timing of the spring bloom in the Labrador Sea. *Marine Ecology Progress Series*, **355**, 9–20, doi:10.3354/meps07233.

Yashayaev, I., 2007: Hydrographic changes in the Labrador Sea, 1960–2005. *Progress in Oceanography*, **73 (3)**, 242–276, doi:10.1016/j.pocean.2007.04.015.

Yashayaev, I., and J. W. Loder, 2016: Recurrent replenishment of Labrador Sea Water and associated decadal-scale variability. *Journal of Geophysical Research: Oceans*, **121 (11)**, 8095–8114, doi:

10.1002/2016JC012046.

Yashayaev, I., and J. W. Loder, 2017: Further intensification of deep convection in the Labrador Sea in 2016. *Geophysical Research Letters*, **44 (3)**, 1429–1438, doi:10.1002/2016GL071668.

Yashayaev, I., I. Peterson, and Z. Wang, 2022: Meteorological, Sea Ice, and Oceanographic Conditions in the Labrador Sea during 2020. *DFO Can. Sci. Advis. Sec. Res. Doc.*

Yoder, J. A., D. A. Siegel, and C. Wilson, 2010: Study of Marine Ecosystems and Biogeochemistry Now and in the Future: Examples of the Unique Contributions from Space. *Oceanography*, **23 (4)**, 104–117, doi:10.5670/oceanog.2010.09.

LIST OF TABLES

Table 1. Research cruise, sampling dates, and number of sampling stations for each nutrient (Si: silicate, N: nitrate, P: phosphate) across the AR7W transect. Information was obtained from the GLODAPv2 (Olsen et al. 2016) and Bedford Institute of Oceanography data sets. 59

TABLE 1. Research cruise, sampling dates, and number of sampling stations for each nutrient (Si: silicate, N: nitrate, P: phosphate) across the AR7W transect. Information was obtained from the GLODAPv2 (Olsen et al. 2016) and Bedford Institute of Oceanography data sets.

Cruise	Dates	Year	n_{Si}	n_N	n_P
HUD-1994-008	29 May–5 June	1994	25	0	24
HUD-1995-011	11–16 June	1995	28	28	28
HUD-1996-006	18–25 May	1996	28	28	28
HUD-1997-009	21–28 May	1997	23	23	23
HUD-1998-023	26 June–3 July	1998	25	0	25
HUD-1999-022	1–11 July	1999	43	0	43
HUD-2000-009	24 May–5 June	2000	27	0	24
HUD-2001-022	4–11 June	2001	34	0	34
HUD-2002-032	2–8 July	2002	35	35	0
HUD-2003-038	23–29 July	2003	34	0	34
HUD-2004-016	20–27 May	2004	29	29	29
HUD-2005-016	29 May–3 June	2005	33	33	31
HUD-2006-019	26–31 May	2006	34	34	34
HUD-2007-011	12–21 May	2007	28	28	28
HUD-2008-009	23–29 May	2008	30	30	30
HUD-2009-015	20–26 May	2009	27	27	27
HUD-2010-014	17–24 May	2010	23	23	21
HUD-2011-009	11–22 May	2011	35	35	35
MLB-2012-001	4–12 June	2012	34	34	34
HUD-2013-008	11–19 May	2013	28	0	24
HUD-2014-007	7–15 May	2014	39	39	39
HUD-2015-006	9–16 May	2015	30	30	30
HUD-2016-006	7–15 May	2016	36	36	36
HUD-2018-008	3-9 May	2018	27	27	27

LIST OF FIGURES

Fig. 1. Spatial distribution of the linear trend in chlorophyll-a as seen from (a) SeaWiFS satellite data between 1998 to 2007, (b) NOBM between 1998 to 2007, (c) PISCES between 1998 to 2007 (d) MODIS satellite data between 2008 to 2017, (e) NOBM between 2008 to 2015 and (f) PISCES between 2008 to 2017. 63

Fig. 2. (a) Time series of monthly spatial averages and (b) map of annual mean chlorophyll-a for the Labrador Sea. The regions over which the spatial averages are derived correspond to the black outline in (b). Solid black lines in (a) denote spatial averages with less than 25% missing coverage in the region, while grey dashed lines denote spatial averages where more than 25% of data are missing within the region (due to cloud cover or insufficient light conditions during winter). The vertical lines in (a) denotes the month of May for each year. The time series and map are based on monthly 4 km resolution chlorophyll-a fields using the MODIS sensor and OCI algorithm (obtained from the NASA Ocean Color data center). . 64

Fig. 3. Chlorophyll-a distribution in the Labrador Sea during May of each year from 2003 to 2018. Maps are based on monthly 4 km resolution chlorophyll-a fields using the MODIS sensor and OCI algorithm (obtained from the NASA Ocean Color data center). 65

Fig. 4. April-September mean chlorophyll-a distributions in the Labrador Sea of each year from 2003 to 2018. Maps are based on monthly 4 km resolution chlorophyll-a fields using the MODIS sensor and OCI algorithm (obtained from the NASA Ocean Color data center). . . . 66

Fig. 5. (a) Mean chlorophyll-a and (b) total production evaluated over Labrador Sea as shown in Figure 2b using both satellite data (GlobColour, SeaWiFS, MODIS and VIIRS) and model output (NOBM, PISCES). For annual production three different NPP algorithms (VGPM, CbPM2 and CAFE) are applied to three different satellite products (SeaWiFS, MODIS and VIIRS). In order to allow sufficient spatial coverage and consistency among datasets, only April through September are used for the annual estimates. Top legend applies to both panels. Algorithms are indicated by color and satellite sensors by line and marker style. 67

Fig. 6. Map indicating the sampling of the AR7W transect (magenta line) and the climatological mean surface currents from drifters. Distances from Greenland (in km) denote the gridded section on which AR7W observations are interpolated. 68

Fig. 7. Mean vertical distribution of nitrate (left), phosphate (middle) and silicate (right) obtained from AR7W observations. Interpolated fields are averaged over 1994-2018, with some years missing as indicated in Table 1. Only AR7W observations from cruises that occurred during May-June are used. Isopycnals based on surface potential density (σ_0) are shown as grey contours. Black line denotes the MLD derived from CTD profiles of σ_0 (using a threshold of 0.03 $\mathrm{kg\,m^{-3}}$ relative to the surface). 69

Fig. 8. Annual cycles (i.e., mean climatology) of nitrate (green), phosphate (red) and silicate (blue) concentrations in the Labrador Sea for the upper 20 m along the AR7W transect, excluding the Labrador Shelf (i.e., within 600 km from Greenland; lon < 53°W). Climatologies are compared to the AR7W dataset for May, June and July (square symbols; mean ± 1 standard deviation for 1994-2018). The winter maxima (plus symbols; vertical length of marker denotes ± 1 standard deviation for 1994-2018) were defined as occurring in March and determined as the observed concentration from the AR7W cruise at the depth of the mean winter MLD. 70

Fig. 9. Vertical distribution of nutrient anomalies for (a-c) 2004-2006 and (d-f) 2014-2016. Anomaly concentrations are shown for silicate (top), nitrate (middle) and phosphate (bottom). Only AR7W observations from cruises that occurred during May-June are used. Black line denotes the MLD derived from profiles of potential density (using a density threshold of 0.03 $\mathrm{kg\,m^{-3}}$ relative to the surface). Note the expanded vertical axes in the upper ocean (0-100 m). 71

Fig. 10. Mean vertical distribution of (a) silicate-to-phosphate (Si:P) and (b) nitrate-to-phosphate (N:P) obtained from interpolation of AR7W observations over the upper 1000 m between 2004 and 2016, and the (c, d) 2004-2006 and (e, f) 2014-2016 anomalies. Only AR7W observations from cruises that occurred during May-June are used. 72

Fig. 11. Vertical sections showing the correlation of (a) silicate, (b) nitrate and (c) phosphate with annual mean surface chlorophyll-a concentration over the Labrador Sea. The correlations are computed over the MODIS period (2004-2018), with some years missing as indicated in Table 1. Nutrient fields are subselected from cruises that occurred during May and/or June. Stippling indicates significant correlations with p-value less than 0.05. 73

Fig. 12. Time series of springtime concentrations of nitrate (green), phosphate (red) and silicate (blue) averaged over the upper Labrador Sea (200-800 m). Nutrient fields are subselected from cruises that occurred during May and/or June. 74

Fig. 13. Spatial correlation pattern between silicate concentrations and MLD. In (a) both silicate and MLD are obtained by interpolation of AR7W profiles and subselected for cruises that occurred during May and/or June. The correlations are computed over the period 1998 to 2018, with some years missing as indicated in Table 1. Silicate concentrations across the AR7W transect from each May-June cruise are also correlated with March MLD from (b) HYCOM and (c) GLORYS12v1. 75

Fig. 14. Comparison of MLD along the AR7W transect in May of (a) 2009, (b) 2010, (c) 2013, (d) 2014, (e) 2015), (f) 2016. Grey line shows the MLD from AR7W profiles of potential density (using a density threshold of 0.03 $\mathrm{kg\,m^{-3}}$). MLD data for May from GLORYS12v1 and HYCOM were subsampled to the same coordinates as the AR7W transect. MLD values from Argo are obtained from Holte and Talley (2009), using the density threshold criteria. . . 76

Fig. 15. Winter convection depth in the Labrador Sea plotted along annual mean time series of SSH-based (i.e., second principle component of North Atlantic SSH field) and density-based (i.e., σ_0 at 300 dbar in the central SPG) gyre indices. 77

Fig. 16. Time series of normalized SPG indices. Normalization was done by subtracting the mean and dividing the time series by its standard deviation. The SSH-based gyre index is shown as solid line along with the density-based gyre index (dashed line). The SSH-based gyre index was used to select years of strong and weak gyre strength depending on whether the value of a particular year exceeds the average by more than 1 standard deviation (i.e., index $<$-1 or $>$1). Years of strong and weak SPG strength are marked as red and blue dots, respectively. . 78

Fig. 17. Anomaly distribution of (a-b) silicate concentrations and (c-d) Si:P ratios over the upper 1000 m of the AR7W transect. Anomalies are obtained by averaging years of strong or weak SPG (based on the gyre index exceeding $\pm$1 standard deviation of the average) and subtracting the mean distribution. 79

Fig. 18. Spatial correlation pattern of winter convection depth in the Labrador Sea with (a) silicate, (b) nitrate and (c) phosphate concentrations along the AR7W transect for the period 1994 to

2018. Note that sampling dates for nutrient concentrations are variable over the given time period and therefore upper ocean concentrations likely include seasonal biases. 80

Fig. 19. Time series of silicate concentration in the upper Labrador Sea (blue) and annual mean chlorophyll-a concentration (green) plotted with convection depth (grey bars). Convection depth is significantly correlated ($p < 0.05$) with both silicate ($r = 0.73$) and chlorophyll-a ($r = 0.57$). Annual mean chlorophyll-a is derived from SeaWiFS (1998-2007, dashed line) and MODIS (2003-2018, solid line). 81

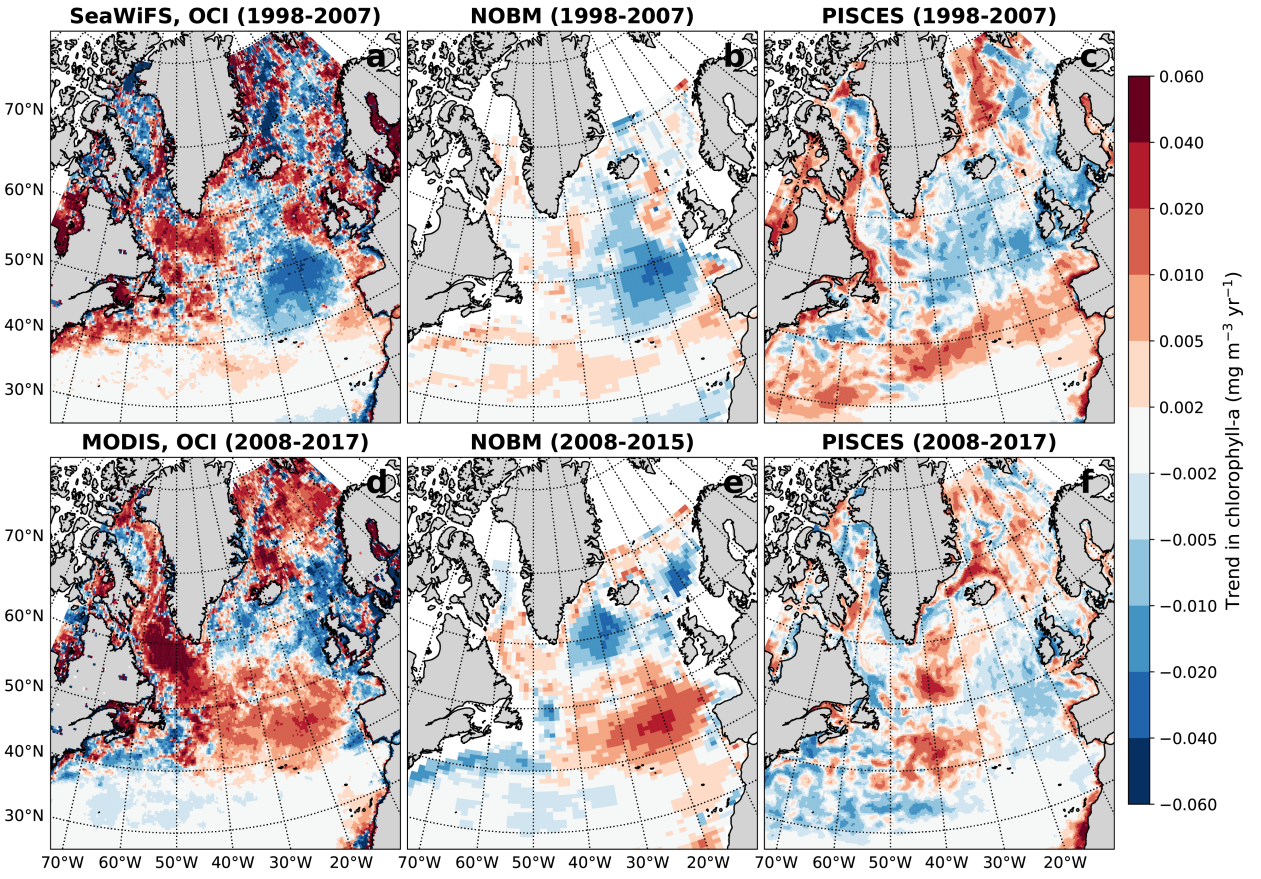

FIG. 1. Spatial distribution of the linear trend in chlorophyll-a as seen from (a) SeaWiFS satellite data between 1998 to 2007, (b) NOBM between 1998 to 2007, (c) PISCES between 1998 to 2007 (d) MODIS satellite data between 2008 to 2017, (e) NOBM between 2008 to 2015 and (f) PISCES between 2008 to 2017.

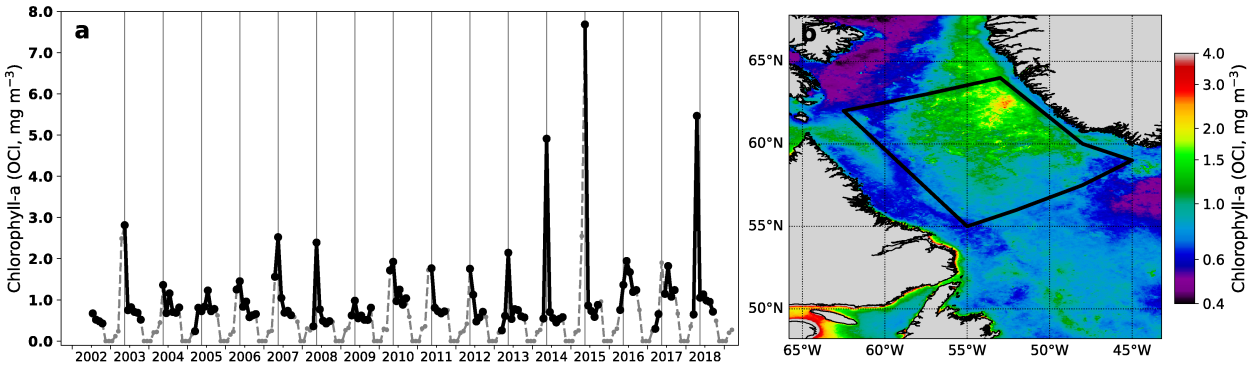

FIG. 2. (a) Time series of monthly spatial averages and (b) map of annual mean chlorophyll-a for the Labrador Sea. The regions over which the spatial averages are derived correspond to the black outline in (b). Solid black lines in (a) denote spatial averages with less than 25% missing coverage in the region, while grey dashed lines denote spatial averages where more than 25% of data are missing within the region (due to cloud cover or insufficient light conditions during winter). The vertical lines in (a) denotes the month of May for each year. The time series and map are based on monthly 4 km resolution chlorophyll-a fields using the MODIS sensor and OCI algorithm (obtained from the NASA Ocean Color data center).

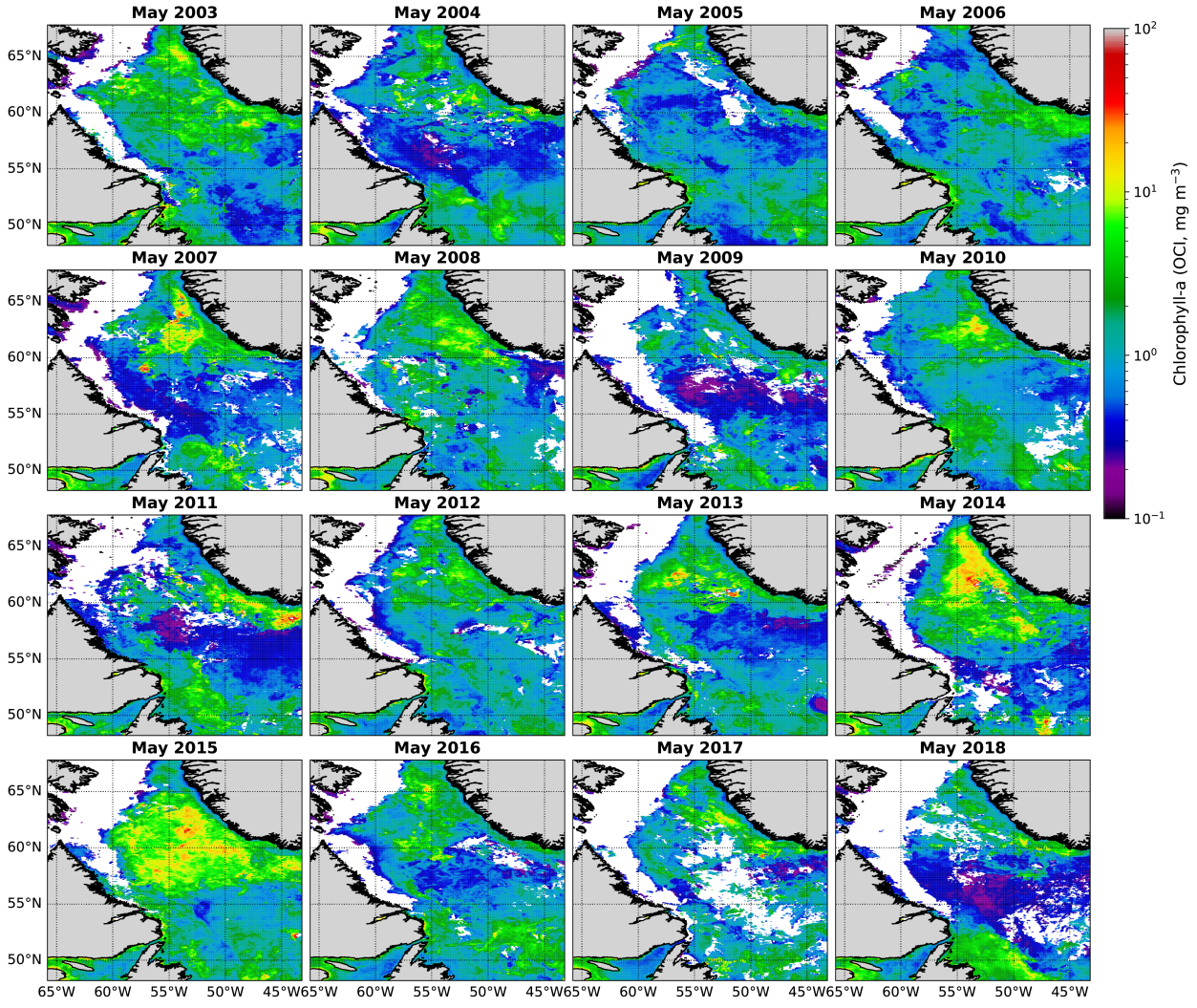

1382 FIG. 3. Chlorophyll-a distribution in the Labrador Sea during May of each year from 2003 to 2018. Maps are
1383 based on monthly 4 km resolution chlorophyll-a fields using the MODIS sensor and OCI algorithm (obtained
1384 from the NASA Ocean Color data center).

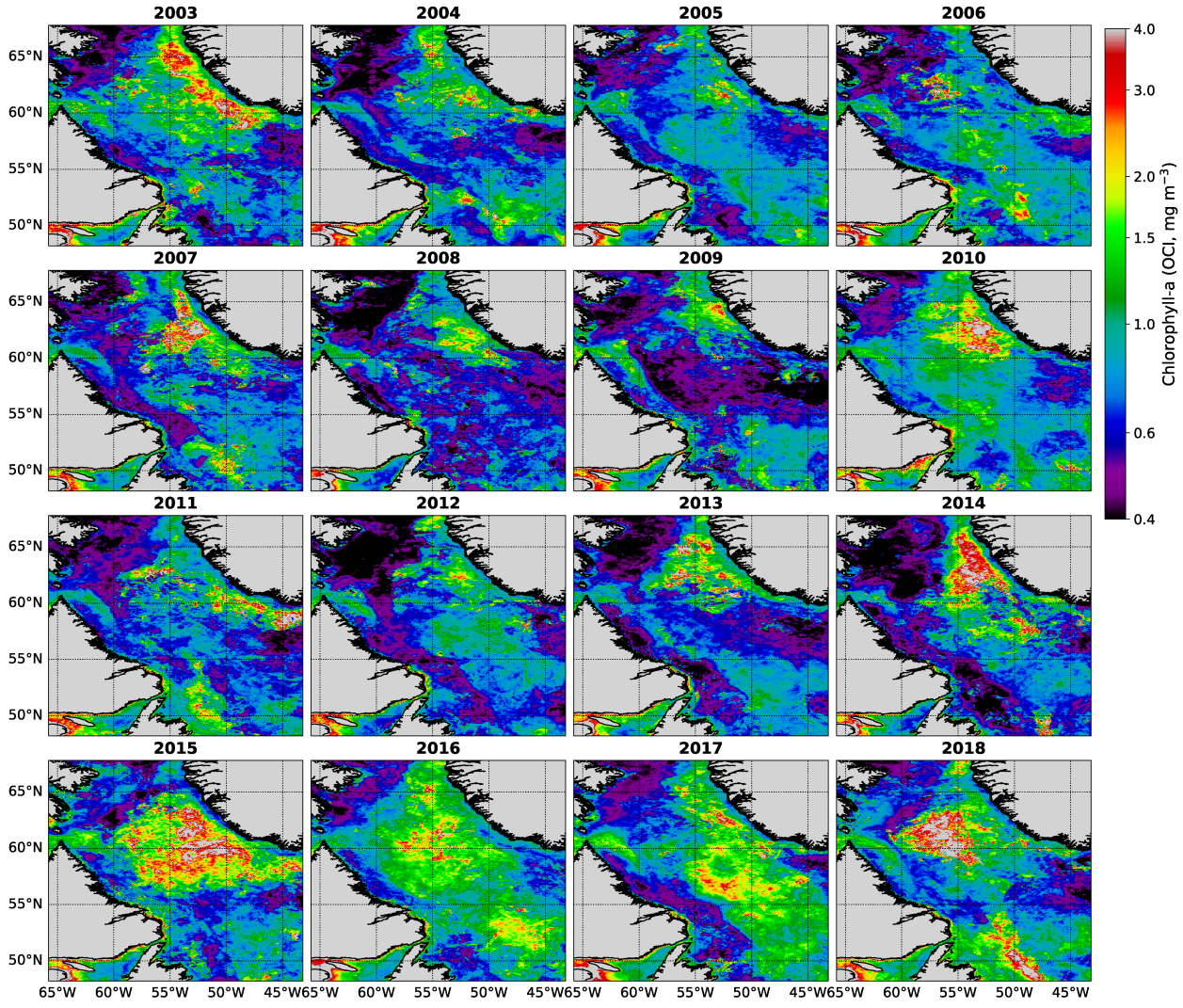

FIG. 4. April-September mean chlorophyll-a distributions in the Labrador Sea of each year from 2003 to 2018. Maps are based on monthly 4 km resolution chlorophyll-a fields using the MODIS sensor and OCI algorithm (obtained from the NASA Ocean Color data center).

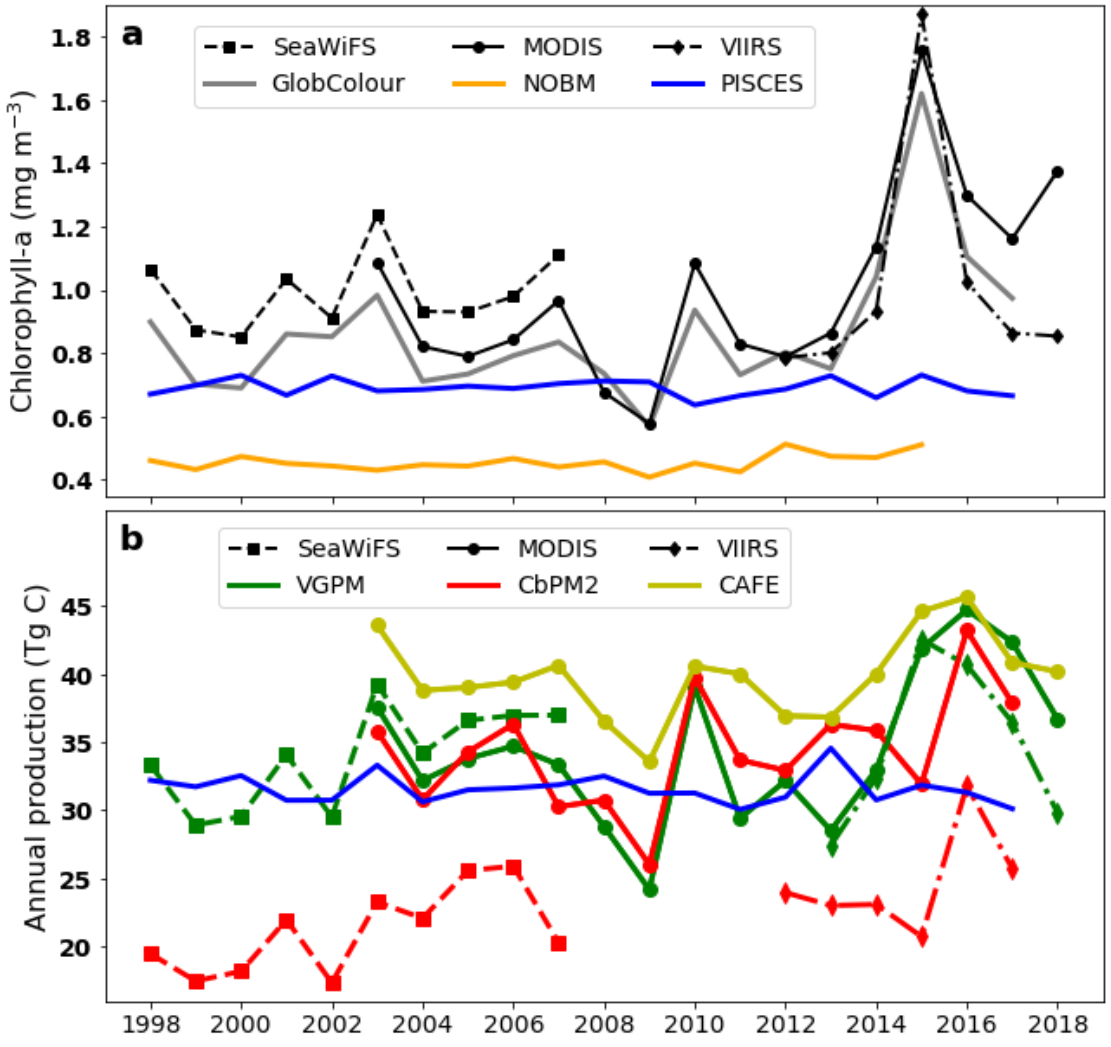

FIG. 5. (a) Mean chlorophyll-a and (b) total production evaluated over Labrador Sea as shown in Figure 2b using both satellite data (GlobColour, SeaWiFS, MODIS and VIIRS) and model output (NOBM, PISCES). For annual production three different NPP algorithms (VGPM, CbPM2 and CAFE) are applied to three different satellite products (SeaWiFS, MODIS and VIIRS). In order to allow sufficient spatial coverage and consistency among datasets, only April through September are used for the annual estimates. Top legend applies to both panels. Algorithms are indicated by color and satellite sensors by line and marker style.

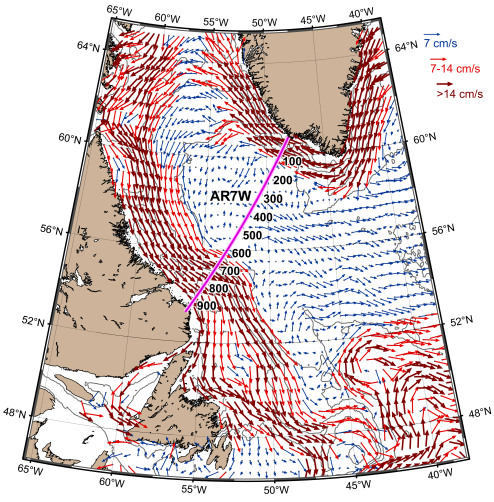

1394 FIG. 6. Map indicating the sampling of the AR7W transect (magenta line) and the climatological mean
1395 surface currents from drifters. Distances from Greenland (in km) denote the gridded section on which AR7W
1396 observations are interpolated.

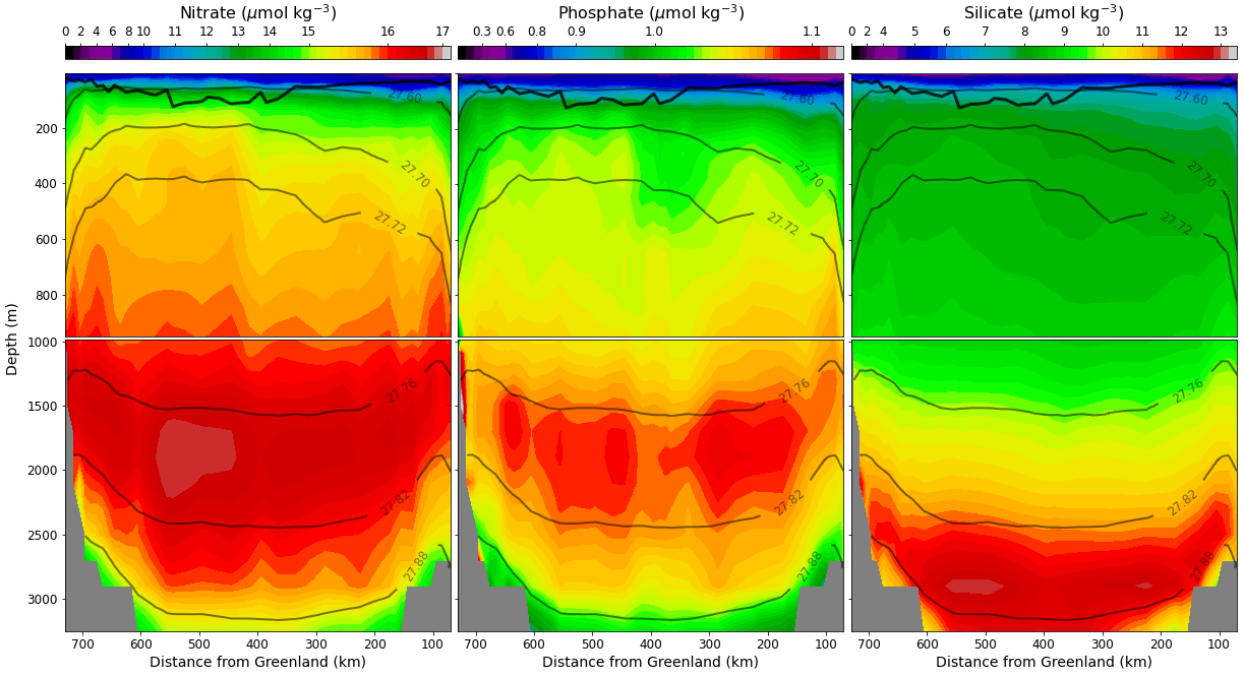

1397 FIG. 7. Mean vertical distribution of nitrate (left), phosphate (middle) and silicate (right) obtained from AR7W
1398 observations. Interpolated fields are averaged over 1994-2018, with some years missing as indicated in Table 1.
1399 Only AR7W observations from cruises that occurred during May-June are used. Isopycnals based on surface
1400 potential density (σ_0) are shown as grey contours. Black line denotes the MLD derived from CTD profiles of σ_0
1401 (using a threshold of 0.03 kg m^{-3} relative to the surface).

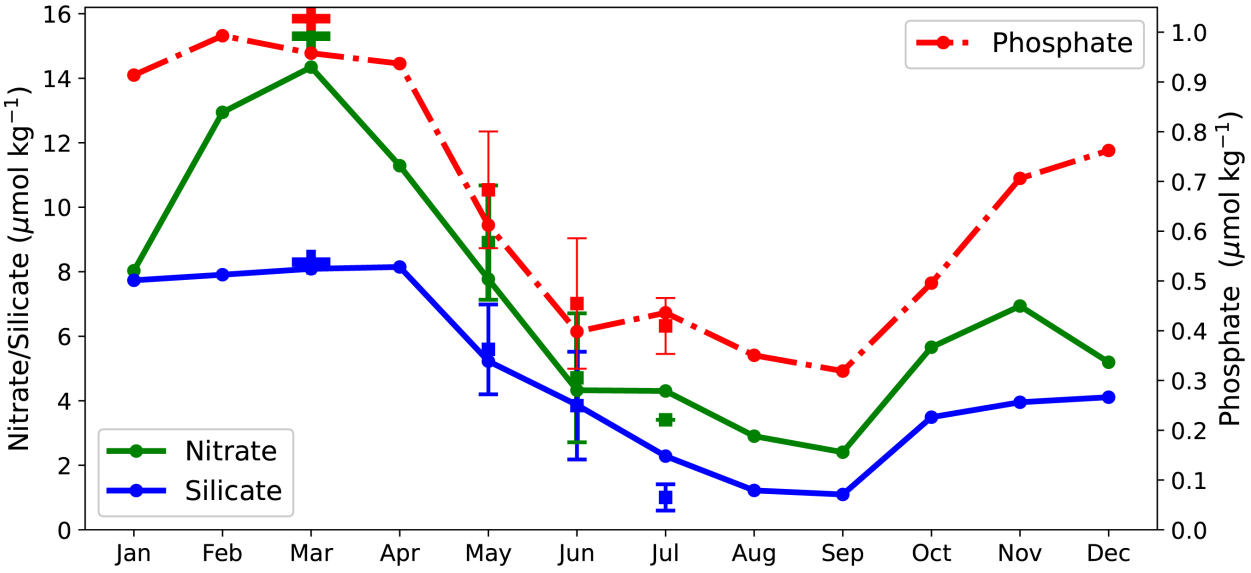

FIG. 8. Annual cycles (i.e., mean climatology) of nitrate (green), phosphate (red) and silicate (blue) concentrations in the Labrador Sea for the upper 20 m along the AR7W transect, excluding the Labrador Shelf (i.e., within 600 km from Greenland; lon < 53°W). Climatologies are compared to the AR7W dataset for May, June and July (square symbols; mean ±1 standard deviation for 1994-2018). The winter maxima (plus symbols; vertical length of marker denotes ±1 standard deviation for 1994-2018) were defined as occurring in March and determined as the observed concentration from the AR7W cruise at the depth of the mean winter MLD.

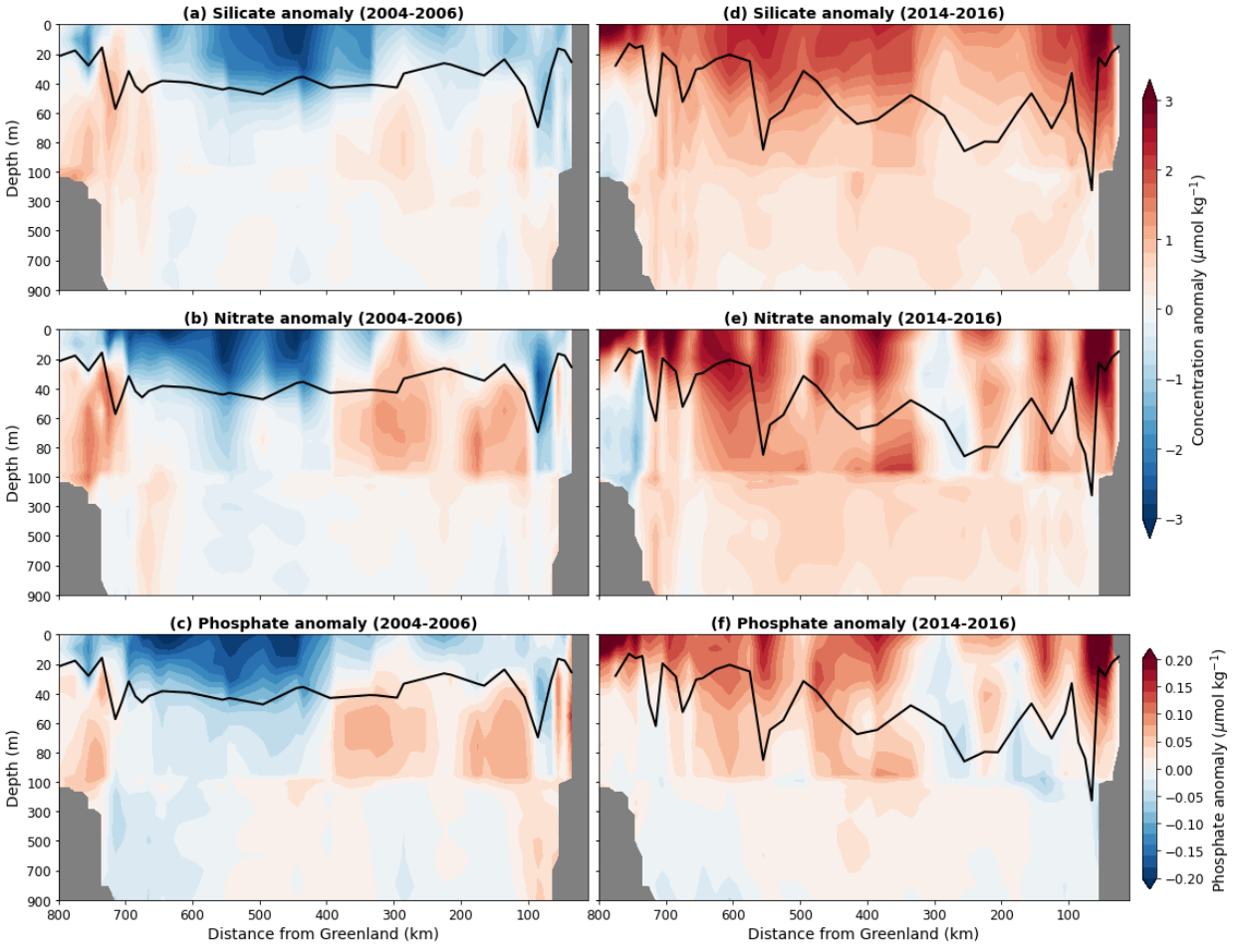

FIG. 9. Vertical distribution of nutrient anomalies for (a-c) 2004-2006 and (d-f) 2014-2016. Anomaly concentrations are shown for silicate (top), nitrate (middle) and phosphate (bottom). Only AR7W observations from cruises that occurred during May-June are used. Black line denotes the MLD derived from profiles of potential density (using a density threshold of 0.03 $\mathrm{kg\,m^{-3}}$ relative to the surface). Note the expanded vertical axes in the upper ocean (0-100 m).

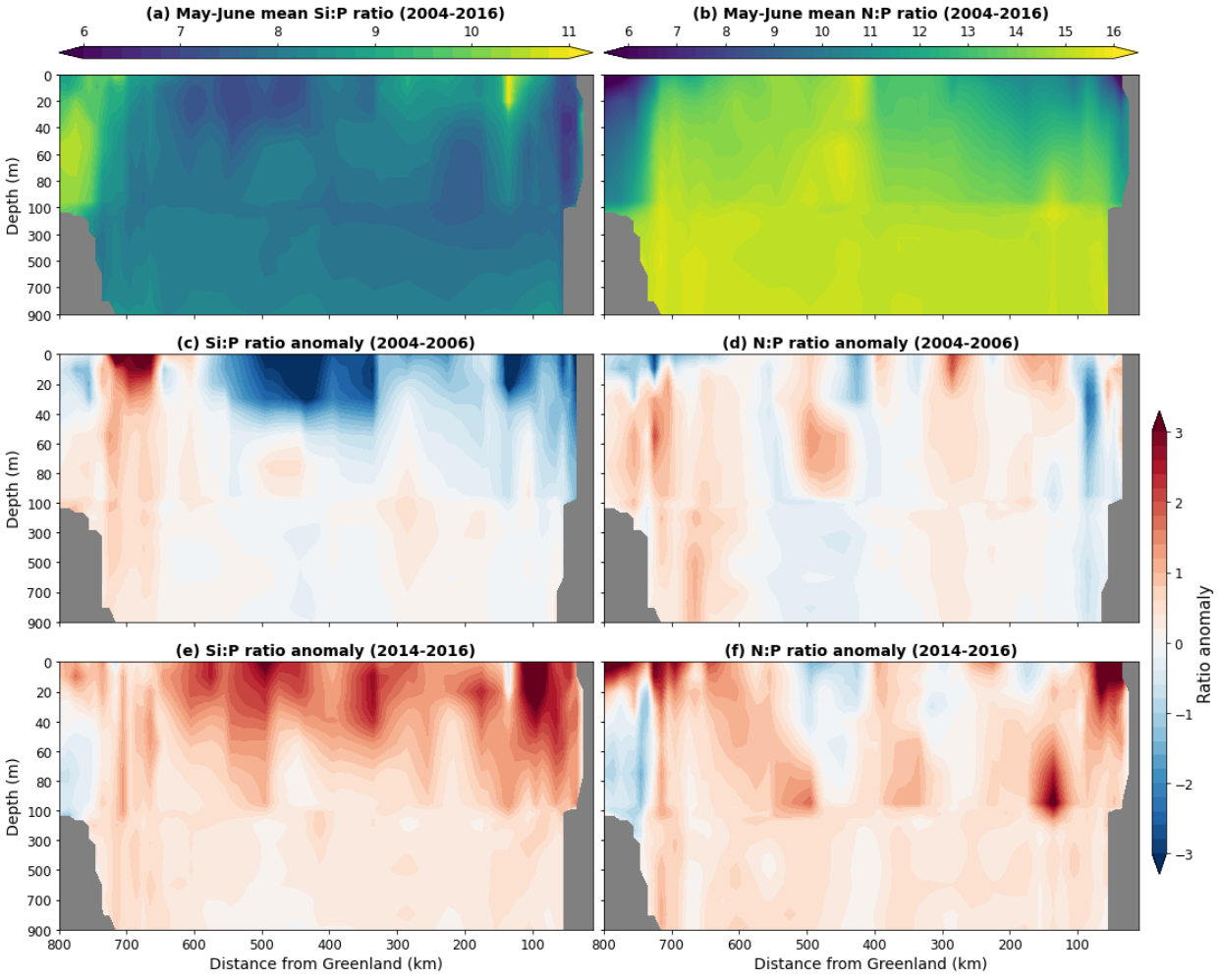

FIG. 10. Mean vertical distribution of (a) silicate-to-phosphate (Si:P) and (b) nitrate-to-phosphate (N:P) obtained from interpolation of AR7W observations over the upper 1000 m between 2004 and 2016, and the (c, d) 2004-2006 and (e, f) 2014-2016 anomalies. Only AR7W observations from cruises that occurred during May-June are used.

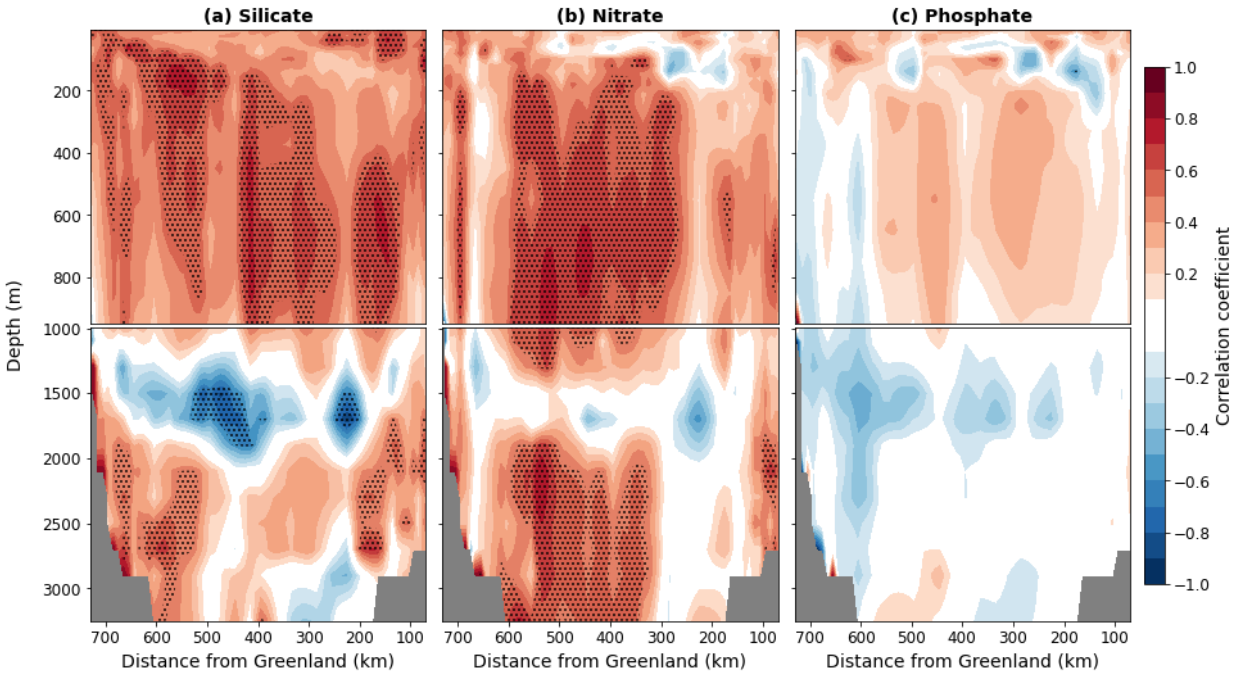

FIG. 11. Vertical sections showing the correlation of (a) silicate, (b) nitrate and (c) phosphate with annual mean surface chlorophyll-a concentration over the Labrador Sea. The correlations are computed over the MODIS period (2004-2018), with some years missing as indicated in Table 1. Nutrient fields are subselected from cruises that occurred during May and/or June. Stippling indicates significant correlations with p-value less than 0.05.

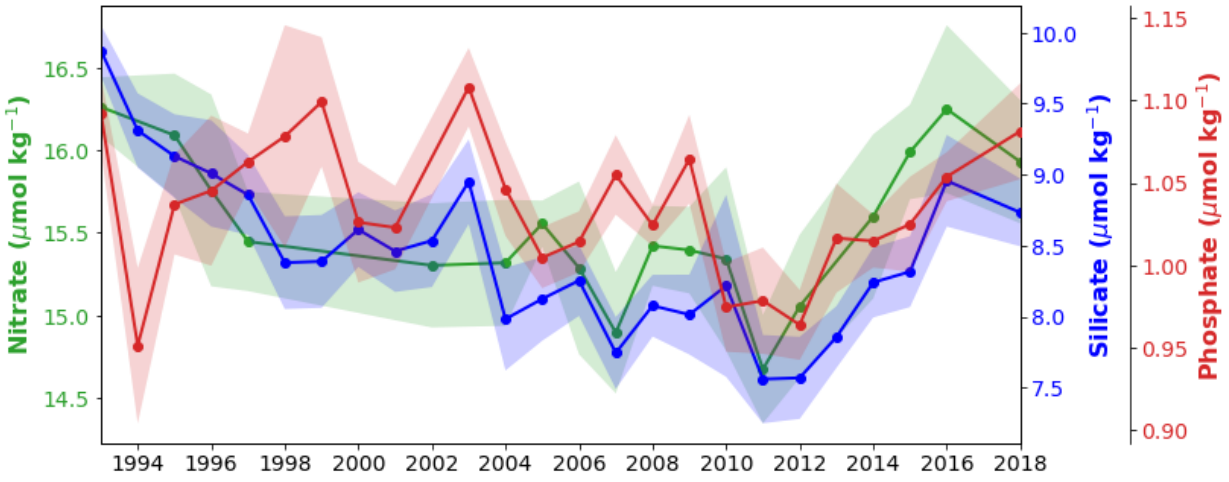

1422 FIG. 12. Time series of springtime concentrations of nitrate (green), phosphate (red) and silicate (blue) aver-
1423 aged over the upper Labrador Sea (200-800 m). Nutrient fields are subselected from cruises that occurred during
1424 May and/or June.

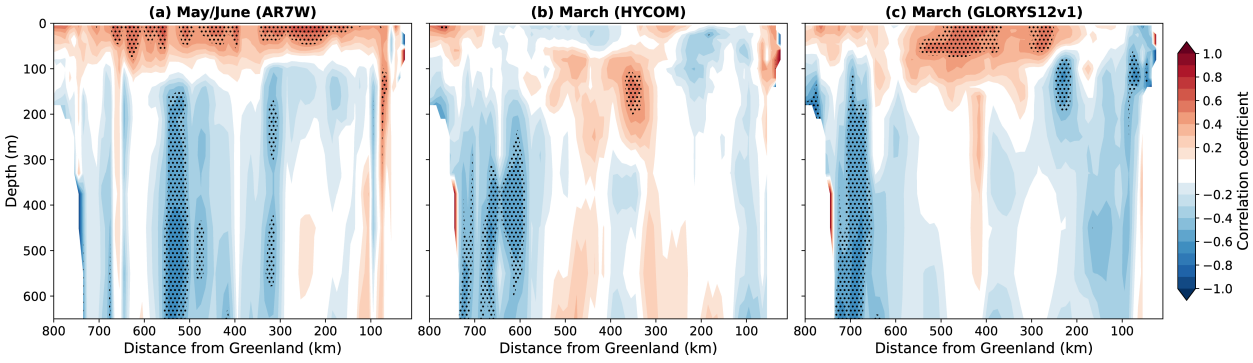

FIG. 13. Spatial correlation pattern between silicate concentrations and MLD. In (a) both silicate and MLD are obtained by interpolation of AR7W profiles and subselected for cruises that occurred during May and/or June. The correlations are computed over the period 1998 to 2018, with some years missing as indicated in Table 1. Silicate concentrations across the AR7W transect from each May-June cruise are also correlated with March MLD from (b) HYCOM and (c) GLORYS12v1.

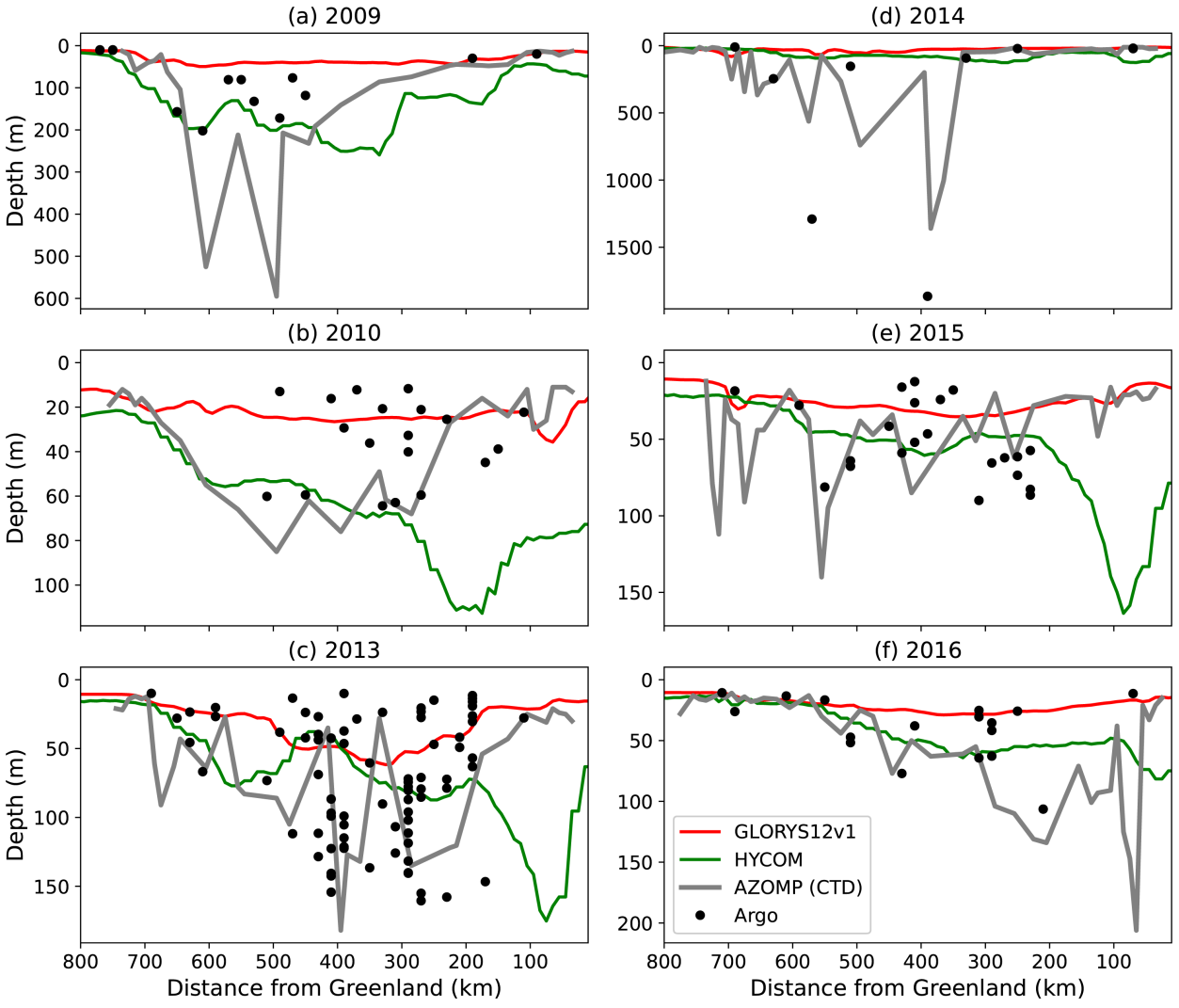

FIG. 14. Comparison of MLD along the AR7W transect in May of (a) 2009, (b) 2010, (c) 2013, (d) 2014, (e) 2015), (f) 2016. Grey line shows the MLD from AR7W profiles of potential density (using a density threshold of 0.03 $\mathrm{kg\,m^{-3}}$). MLD data for May from GLORYS12v1 and HYCOM were subsampled to the same coordinates as the AR7W transect. MLD values from Argo are obtained from Holte and Talley (2009), using the density threshold criteria.

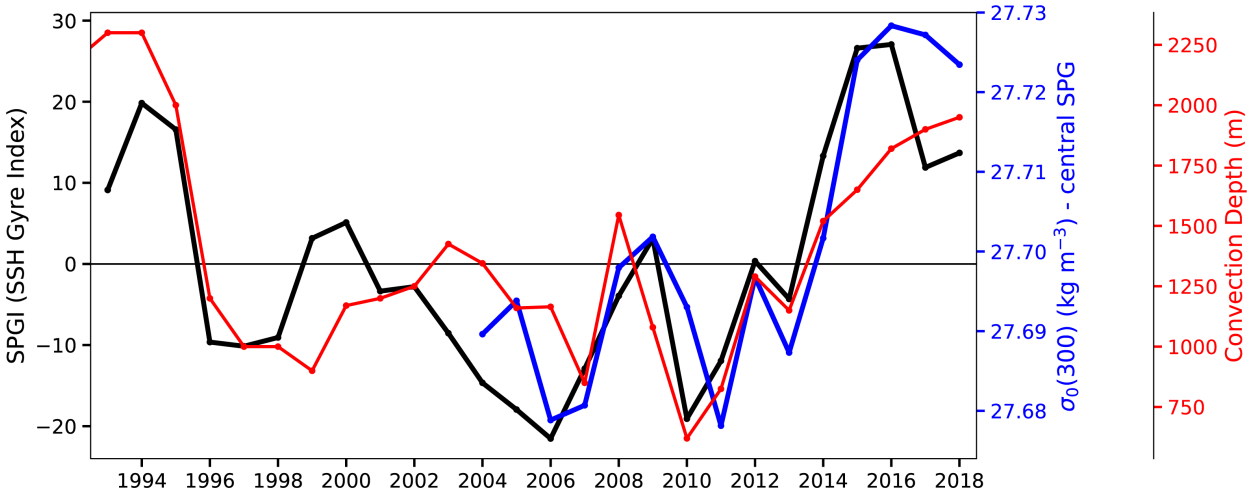

1435 FIG. 15. Winter convection depth in the Labrador Sea plotted along annual mean time series of SSH-based
1436 (i.e., second principle component of North Atlantic SSH field) and density-based (i.e., σ_0 at 300 dbar in the
1437 central SPG) gyre indices.

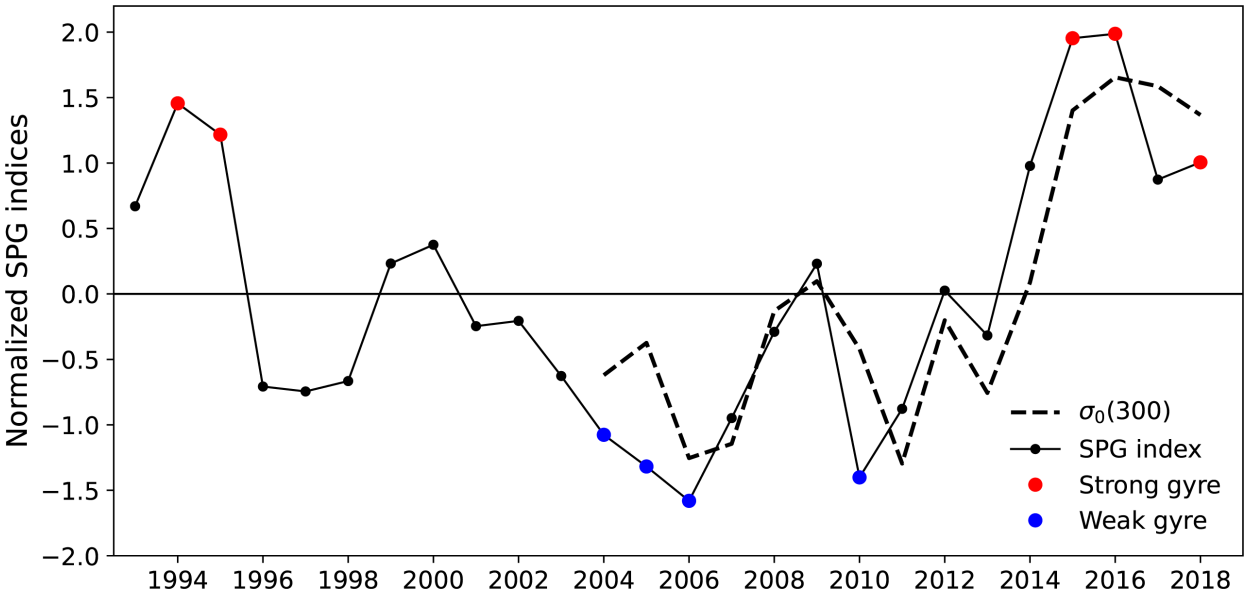

FIG. 16. Time series of normalized SPG indices. Normalization was done by subtracting the mean and dividing the time series by its standard deviation. The SSH-based gyre index is shown as solid line along with the density-based gyre index (dashed line). The SSH-based gyre index was used to select years of strong and weak gyre strength depending on whether the value of a particular year exceeds the average by more than 1 standard deviation (i.e., index $<$-1 or $>$1). Years of strong and weak SPG strength are marked as red and blue dots, respectively.

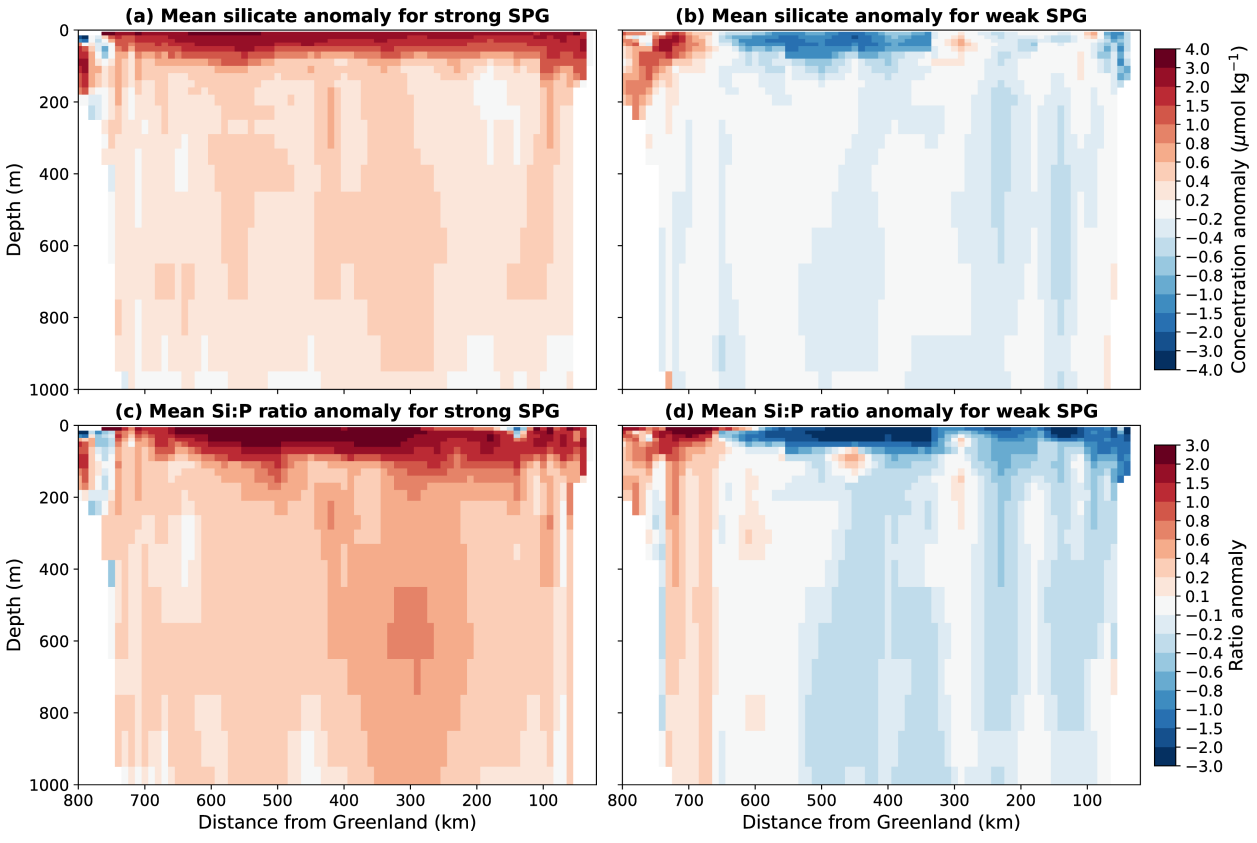

1444 FIG. 17. Anomaly distribution of (a-b) silicate concentrations and (c-d) Si:P ratios over the upper 1000 m of
1445 the AR7W transect. Anomalies are obtained by averaging years of strong or weak SPG (based on the gyre index
1446 exceeding ± 1 standard deviation of the average) and subtracting the mean distribution.

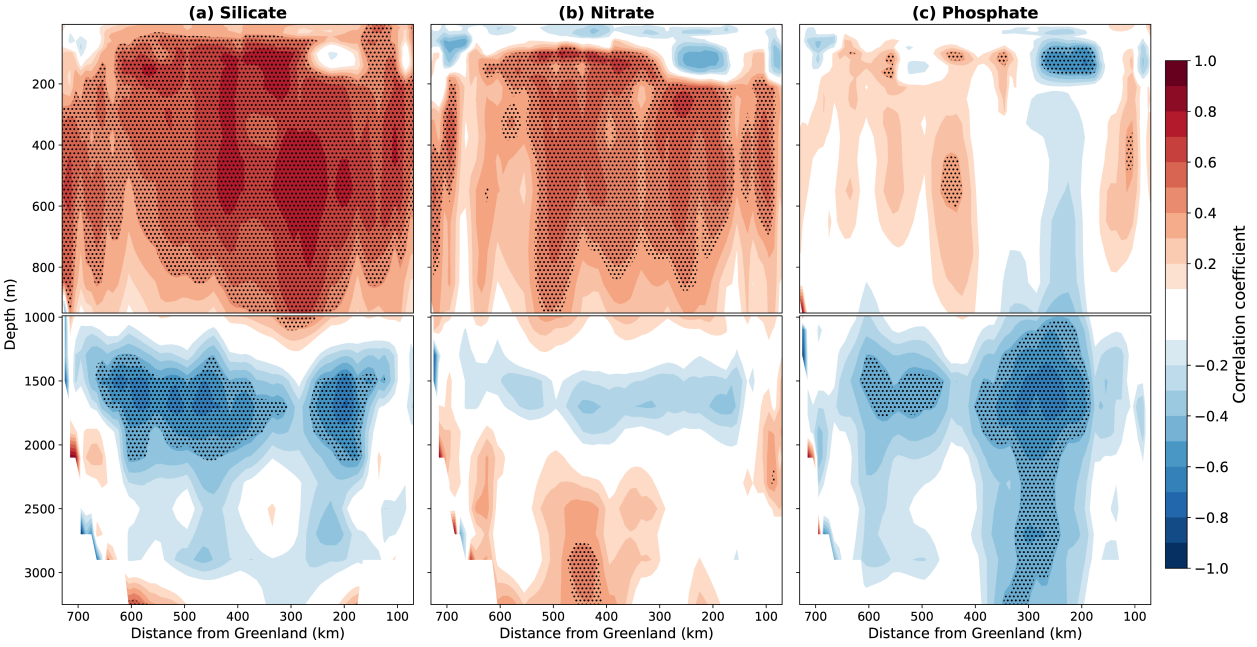

FIG. 18. Spatial correlation pattern of winter convection depth in the Labrador Sea with (a) silicate, (b) nitrate and (c) phosphate concentrations along the AR7W transect for the period 1994 to 2018. Note that sampling dates for nutrient concentrations are variable over the given time period and therefore upper ocean concentrations likely include seasonal biases.

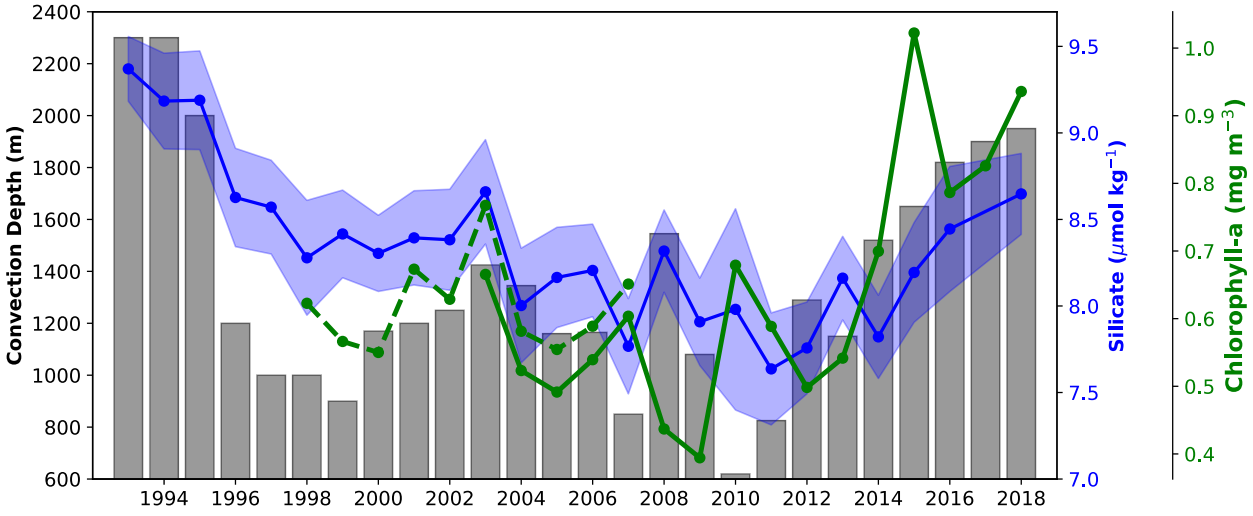

FIG. 19. Time series of silicate concentration in the upper Labrador Sea (blue) and annual mean chlorophyll-a concentration (green) plotted with convection depth (grey bars). Convection depth is significantly correlated ($p < 0.05$) with both silicate ($r = 0.73$) and chlorophyll-a ($r = 0.57$). Annual mean chlorophyll-a is derived from SeaWiFS (1998-2007, dashed line) and MODIS (2003-2018, solid line).